Available online at www.sciencedirect.com

ScienceDirect

Geochimica et Cosmochimica Acta 307 (2021) 168–191

Geochimica et Cosmochimica Acta

www.elsevier.com/locate/gca

# Temporal evolution of $\delta^{44/40}$Ca and $^{87}$Sr/$^{86}$Sr of carbonatites: Implications for crustal recycling through time

Anupam Banerjee [a,1], Ramananda Chakrabarti [a,*], Antonio Simonetti [b]

[a] Centre for Earth Sciences, Indian Institute of Science, Bangalore, India
[b] Department of Civil and Environmental Engineering and Earth Sciences, University of Notre Dame, Notre Dame, IN, USA

Received 12 October 2020; accepted in revised form 22 May 2021; Available online 2 June 2021

**Abstract**

Carbonatites are igneous rocks composed of over 50% modal carbonate minerals and their exact origin and possible mode (s) of formation are still debated. We report stable Ca isotopic compositions ($\delta^{44/40}Ca_{SRM915a}$) of globally distributed carbonatites ($n = 46$) from 22 different locations ranging in age from 2.61 Ga to recent along with their major, trace element concentrations and $^{87}$Sr/$^{86}$Sr ratios. The $\delta^{44/40}Ca_{SRM915a}$ values for carbonatites older than 300 Ma, except for four samples from the Neoproterozoic south Indian carbonatites and the Phalaborwa complex of South Africa, display limited variation (~0.18‰, $n = 12$) with $\delta^{44/40}$Ca values overlapping (given their associated analytical uncertainties) with the estimated $\delta^{44/40}Ca_{SRM915a}$ value of the bulk silicate Earth (BSE, 0.94 ± 0.10‰). The $^{87}Sr/^{86}Sr_{(t)}$ of these samples (0.70149–0.70394) are consistent with derivation from a depleted mantle source with a time-integrated Rb/Sr ratio of ~0.017. In contrast, carbonatites with emplacement ages younger than 300 Ma display much wider variations in $\delta^{44/40}$Ca values (0.63‰, $n = 29$) with sixteen samples displaying values lower than that for the BSE and radiogenic $^{87}$Sr/$^{86}$Sr compositions (0.70313–0.71044). The low $\delta^{44/40}$Ca values for the younger carbonatites are consistent with the presence of recycled crustal carbonates, with compositions similar to those of 100–200 Ma and 400–500 Ma old carbonates, in their mantle source, which is also consistent with their radiogenic $^{87}$Sr/$^{86}$Sr ratios. Model calculations, based on $\delta^{44/40}$Ca and $^{87}Sr/^{86}Sr_{(t)}$ ratios for mantle peridotite and eclogite sources and marine carbonates of different ages, suggest that the $\delta^{44/40}$Ca and $^{87}$Sr/$^{86}$Sr for most young carbonatites (<300 Ma) examined here can be explained by the presence of <10 wt% recycled crustal carbonates in their mantle source.

The contrasting Ca and Sr isotope compositions between younger (<300 Ma) and older (>300 Ma) carbonatites may reflect changing geodynamic conditions. The prevalent Ca and Sr isotope signatures attributed to crustal recycling that is observed in carbonatites younger than 300 Ma most likely reflect two global-scale processes: (i) an increased amount of subduction flux due to high convergence rates subsequent to the break-up of the Pangea supercontinent, and (ii) greater amount of plume activity during the last 300 million years of Earth history. Additionally, the low $\delta^{44/40}$Ca values of younger carbonatites could have been accentuated by subduction of marine carbonates (aragonitic) with relatively low $\delta^{44/40}$Ca. In contrast to the younger carbonatites, Ca and Sr isotope compositions for the carbonatites older than 300 Ma investigated here suggest that crustal recycling was much more sporadic in the Precambrian.


*Keywords:* Global carbonatites; Calcium stable isotopes; Radiogenic strontium isotopes; Crustal carbonate recycling; Mantle geodynamics

## 1. INTRODUCTION

Carbonatites are unique igneous rocks with >50% modal carbonate minerals. A mantle origin for carbonatite

* Corresponding author.
*E-mail addresses:* ramananda@iisc.ac.in, ramananda@gmail.com (R. Chakrabarti).
[1] Present address: Department of Geology, Faculty of Science, Niigata University, Japan.

https://doi.org/10.1016/j.gca.2021.05.046
0016-7037/

melts has been advocated by several studies on the basis of their radiogenic, stable, and noble gas isotope compositions (e.g., Bell and Simonetti, 2010), and presence of carbonatite melt inclusions within kimberlitic diamond (Kaminsky et al., 2016). As it is the most carbon(ate) rich terrestrial igneous rock, studies of carbonatites provide important understanding of the nature and source of mantle carbon, recycling of surface carbon, and essentially the global carbon cycle. Carbonatite melts are characterized by extremely low viscosity, density, and low temperature, factors that favour a rapid rise of these magmas through overlying crust and hence minimizes melt-crust interaction time (Dobson et al., 1996; Jones et al., 2013). Therefore, the likelihood is high that carbonatite magmas transit through the crust without significant contamination, especially for elements like Ca, Sr, and the REEs, which are enriched in carbonatitic melts. Carbonatites are relatively rare with approximately 527 global occurrences; however, they are found on all the continents and range in age from Archean to present (Woolley and Church, 2005; Woolley and Kjarsgaard, 2008). Given their broad temporal and spatial occurrences, radiogenic (Nd, Pb, Sr, Hf) and stable (Li, B, Ba) isotopic compositions of carbonatites have been used to understand the secular evolution of Earth's upper mantle (Bell and Blenkinsop, 1987; Bizzarro et al., 2002; Halama et al., 2008; Rukhlov et al., 2015; Hulett et al., 2016; Li et al., 2020).

Radiogenic Sr, Nd, Pb, and Hf isotopic studies have suggested that many carbonatites with different temporal and spatial distributions are genetically linked with mantle plumes (Simonetti et al., 1998; Bizzarro et al., 2002; Srivastava et al., 2005; Ernst and Bell, 2010; Chandra et al., 2019). In contrast, numerous young carbonatites (<200 Ma) show isotopic compositions similar to those of ocean island basalts (OIBs) and define a Nd-Sr isotope array representing a possible mixing between HIMU and EMI mantle end-members (Nelson et al., 1988; Simonetti et al., 1995; Bell and Tilton, 2001; Hoernle et al., 2002; Bizimis et al., 2003; Srivastava et al., 2005; Bell and Simonetti, 2010). The $\delta^{13}C_{PDB}$ (ranging from 2.8 to −6.5‰) and $\delta^{18}O_{SMOW}$ (ranging from 5 to 25‰) compositions for carbonatites worldwide indicate that they are primarily mantle-derived with some showing signatures that may be attributed to the presence of possible recycled inorganic carbon in their mantle source region (Simonetti et al., 1995; Ray et al., 1999; Srivastava et al., 2005; Ray and Ramesh, 2006; Bell and Simonetti, 2010). However, $\delta^{13}C_{PDB}$ and $\delta^{18}O_{SMOW}$ values for carbonatites are also found to be significantly modified by low temperature alteration processes during or after emplacement (e.g., Simonetti et al., 1995; Hoernle et al., 2002; Ray and Ramesh, 2006; Zaitsev and Keller, 2006). Stable Li and Ba isotope compositions of global carbonatites record relatively limited variations ($\delta^{7}Li = 4.1 \pm 1.3‰$ and $\delta^{137/134}Ba = -0.03$ to 0.09‰, respectively) and most of them overlap with estimated mantle compositions ($\delta^{7}Li$= ~1–6‰ and $\delta^{137/134}Ba$= +0.05 ± 0.06‰, respectively) (Halama et al., 2008; Li et al., 2020). In contrast, stable B isotopic compositions for carbonatite samples worldwide show significant variations (Hulett et al., 2016; Cimen et al., 2018, 2019; Kuebler et al., 2020). Carbonatite samples older than 300 Ma exhibit $\delta^{11}B$ values overlapping with (depleted) asthenospheric-like mantle (−7.1 ± 0.9‰; Marschall et al., 2017); however, samples younger than 300 Ma display a much broader range and more positive $\delta^{11}B$ values, suggesting significant contributions from recycled (subducted crustal) materials (Hulett et al., 2016). The isotopes of these minor/trace elements (B, Li, Ba) are powerful tracers of crustal recycling, but these elements could be hosted within multiple types of subducted material such as terrigenous, pelagic, and/or carbonate sediments. The present study focuses on the isotopes of calcium, which is one of the major elements of carbonatite magmas, to investigate the origin of carbon(ates) in carbonatites and evaluate the temporal evolution of Earth's upper mantle.

Calcium, with six naturally occurring isotopes ($^{40}Ca$, $^{42}Ca$, $^{43}Ca$, $^{44}Ca$, $^{46}Ca$ and $^{48}Ca$), is one of the most abundant major elements in carbonatites. Due to the large relative mass difference (~20%) between its lightest ($^{40}Ca$) and heaviest ($^{48}Ca$) stable isotopes, Ca isotopes are expected to show significant stable isotopic fractionation. Stable Ca isotopic compositions are reported relative to the NIST SRM915a standard using the delta notation where $\delta^{44/xy}Ca_{SRM915a}$ is defined as $(((^{44}Ca/^{xy}Ca_{Sample})/(^{44}Ca/^{xy}Ca_{SRM915a}) - 1) * 1000$ and xy is either mass 40 or mass 42. The $\delta^{44/40}Ca_{SRM915a}$ of the upper mantle was first estimated to be 1.05 ± 0.04‰, based on the $\delta^{44/40}Ca$ values of ortho- and clinopyroxene and their modal proportions in the upper mantle peridotites (Huang et al., 2010a). The $\delta^{44/40}Ca_{SRM915a}$ value of the bulk silicate Earth (BSE) was further refined to 0.94 ± 0.05‰ based on analyses of garnet- and spinel-bearing fertile mantle peridotites (Kang et al., 2017), and more recently to 0.94 ± 0.10‰ based on analyses for a large number of mantle lherzolites and harzburgites as well as fertile mantle rocks from different geological settings (Chen et al., 2019). In contrast to the limited variations in $\delta^{44/40}Ca$ values of pristine mantle-derived rocks (c.f., Antonelli and Simon, 2020), marine carbonates display larger ranges in $\delta^{44/40}Ca$, with values generally lower than the BSE (Fig. A. 1a) (c.f., Farkaš et al., 2007a, b; Fantle and Tipper, 2014; Blättler and Higgins, 2017; Zhu et al., 2020a). The low $\delta^{44/40}Ca$ values are dominantly observed in Phanerozoic carbonates while Precambrian carbonates, typically show higher, BSE-like $\delta^{44/40}Ca$, although significant variations are observed for Precambrian carbonates within certain periods of geologic time (Fig. A. 1b). The contrasting $\delta^{44/40}Ca$ values between those for mantle-derived rocks and crustal carbonates suggest that Ca isotopes may be used as a potential tracer of recycled crustal carbonates and have been widely used in tracking recycled components in plume-derived basalts (Huang et al., 2011) and calc-alkaline volcanic rocks (Liu et al., 2017), as well as tracing mantle metasomatism (Kang et al., 2017; Zhao et al., 2017; Chen et al., 2019; Ionov et al., 2019; Kang et al., 2020). Calcium stable isotopic studies of carbonatites are limited. The $\delta^{44/40}Ca$ of carbonatite samples from the ~65 Ma old Ambadongar carbonatite complex (India), associated with the Deccan volcanic province, indicates the presence of ~160 million year old recycled carbonates in the Réunion plume source

(Banerjee and Chakrabarti, 2019). More recently, Amsellem et al. (2020) reported stable Ca isotopic compositions of globally distributed carbonatites and interpreted the low $\delta^{44/40}Ca_{SRM915a}$ of carbonatites (0.07–0.82‰, average of 0.26 ± 0.25‰, 2SD, ($n$ = 50); converted from $\delta^{42/44}Ca$ measurements obtained by MC-ICP-MS) to suggest the presence of recycled carbonates in their mantle source regions irrespective of their emplacement ages.

However, the $\delta^{44/40}Ca$ values of carbonatites reported by Amsellem et al. (2020) are significantly lower than the $\delta^{44/40}Ca$ of carbonatites from the Deccan volcanic province of India (Banerjee and Chakrabarti, 2019), those of oceanic carbonatites from the Cape Verde and the Canary Islands (Amini et al., 2009) and the USGS carbonatite rock standard COQ-1 (from the Oka carbonatite complex of Canada) (Feng et al., 2017; He et al., 2017; Li et al., 2018; Liu et al., 2019). Additionally, the unusually low $\delta^{44/40}Ca$ values of many of these carbonatites (Amsellem et al., 2020) are lower than those of crustal carbonates (Farkaš et al., 2007a, b; Fantle and Tipper, 2014; Blättler and Higgins, 2017; Zhu et al., 2020a), which leads to mass-balance related complications in interpreting the data. The mixing model between mantle and carbonate endmembers used by Amsellem et al. (2020) also assumes that $\delta^{44/40}Ca$ exchange happens independent of Ca exchange and the end member values chosen for this modelling are arbitrary.

In contrast to the interpretation of Amsellem et al. (2020), a recent Ca isotopic study of global carbonatites by Sun et al. (2021) suggests that recycled carbonates do not play any role in controlling the Ca isotopic compositions of carbonatites; they report relatively heavy $\delta^{44/42}Ca_{SRM915a}$ values for global carbonatites (0.26–0.59‰), measured using MC-ICPMS, which when converted to $\delta^{44/40}Ca_{SRM915a}$ values, assuming equilibrium or kinetic fractionation, range from 0.53 to 1.21‰ and 0.54–1.24‰, respectively. The Ca isotopic compositions of 'primary carbonatites', not affected by hydrothermal alteration, are however lower than the Ca isotopic composition of the bulk silicate Earth; these lower Ca isotopic compositions are controlled by partial melting processes of the mantle and are not attributable to carbonate recycling (Sun et al., 2021). Interestingly, many of the samples classified as 'non-primary' carbonatites, based on their Ca and C isotopic compositions, are characterized by Ca isotopic compositions that overlap with those of 'primary' carbonatites. Overall, the contrasting Ca isotopic compositions reported for globally distributed carbonatites from both previous studies using a MC-ICPMS approach (Amsellem et al., 2020; Sun et al., 2021) has resulted in postulating contrasting interpretations, and therefore a re-evaluation of the $\delta^{44/40}Ca$ signatures for carbonatites employing a different methodology (double spike-thermal ionization mass spectrometry- DS-TIMS) as adopted here is essential.

This study reports the stable Ca isotopic compositions for 46 carbonatites from 22 occurrences worldwide that range in age from 2.61 Ga to recent. Also reported are the major and selected trace element concentrations and Sr isotope data for the same samples. Among these 46 carbonatite samples, data for six samples, associated with the Deccan volcanic province, have been reported earlier (Banerjee and Chakrabarti, 2019). The combined Ca (and Sr) isotopic compositions for these globally distributed carbonatite samples are interpreted in terms of varying amounts of carbonate recycling through time as well as changes in the compositions of recycled material, which has implications for mantle geodynamics.

## 2. SAMPLES AND ANALYTICAL METHODS

The samples used in this study include calcite separates ($n$ = 17) from different carbonatites worldwide that were earlier analysed for their boron isotopic composition (Hulett et al., 2016) and whole rock (WR) carbonatite samples ($n$ = 23). Also included are six WR- carbonatite samples associated with the eruption of the Deccan Traps, which have been studied for their geochemical, Nd, Sr, and Ca isotopic compositions (Banerjee and Chakrabarti, 2019). Among these 46 carbonatites, 16 samples were collected from 10 different geographic locations and have emplacement ages older than 300 Ma, whereas the remaining 30 samples are from 12 different geographic locations and have emplacement ages younger than 300 Ma (Fig. 1). All the carbonatites investigated in this study have been previously characterized in terms of their petrology, geochemical, and radiogenic and stable isotopic compositions, and the samples analysed in this study do not exhibit any visible signs of surface alteration. Additional details on the petrogenetic history of the carbonatites studied here, including published isotopic compositions, are summarized in the Supplementary Table A.1.

Analytical procedures used for the measurements of major and trace element concentrations are explained in detail in earlier studies (Banerjee et al., 2016; Banerjee and Chakrabarti, 2019). Briefly, ~25 mg of powdered WR samples were dissolved using a 1:3 mixture of concentrated HF and $HNO_3$ for approximately five to six hours in 15 ml screw-cap, flat-base Teflon vials (Savillex, USA) with frequent ultrasonication and the solution was carefully monitored to avoid formation of $CaF_2$. Upon evaporation of the HF-$HNO_3$ mixture, samples were further treated with a 1:1 mixture of concentrated HCl and $HNO_3$ for at least 24 h. Calcite separates from carbonatites were dissolved using a 1:2 mixture of concentrated HCl and $HNO_3$ for 24 h. Upon evaporation of HCl and $HNO_3$ mixtures, both WR carbonatites and the calcite separates were diluted ~4000 and ~10,000 times using 2% $HNO_3$ (v/v) for measurements of trace element and major element concentrations, respectively. Elemental concentrations were measured using a Thermo Scientific X-Series II quadrupole inductively coupled plasma mass spectrometer (ICPMS) at the Centre for Earth Sciences (CEaS), Indian Institute of Science (IISc), Bangalore. USGS rock standards BCR-2 (Columbia river basalt) and BHVO-2 (Hawaiian basalts) were used as calibration standards whereas AGV-2 (Guano valley andesite) and COQ-1 (carbonatite) were measured as 'unknowns' along with the samples to monitor the accuracy and precision of the measurements. The silicate rock standards BCR-2, BHVO-2 and AGV-2 were dissolved using a 1:1 mixture

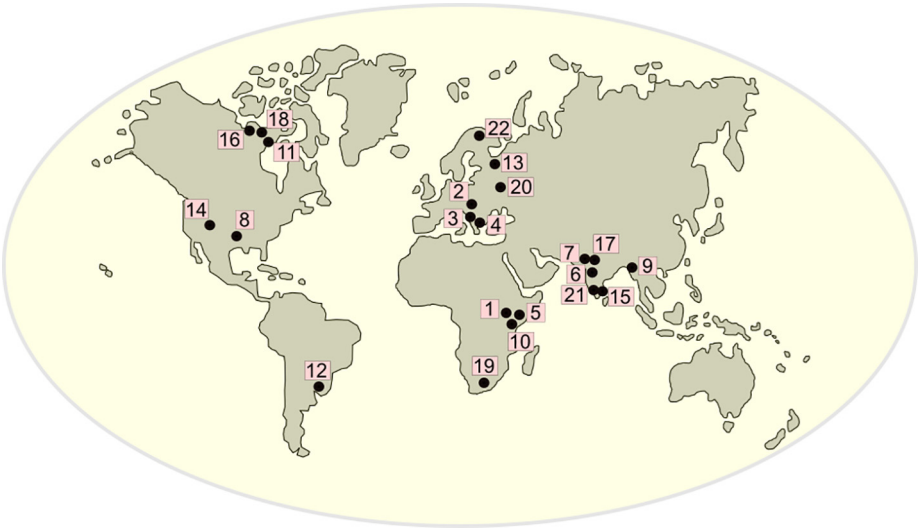


Fig. 1. A schematic representation of the world map showing the geographic locations of the carbonatites analysed in the present study. Numbers in the figure correspond to the following carbonatite occurrences: 1- Kalyango, Uganda; 2-Polino, Italy; 3-Vallone Toppo, Italy; 4-Kaiserstuhl, Germany; 5-Sukulu, Uganda; 6-Ambadongar, India; 7-Barmer, India; 8-Magnet Cove, USA; 9-Sung Valley, India; 10-Panda Hill, Tanzania; 11-Oka, Canada; 12-Jacupiranga, Brazil; 13-Kovdor, Russia; 14-Iron Hill, USA; 15-Sevathur, Onnakara, Garigapalli (southern Indian carbonatite complex); 16-Prairie Lake, Canada; 17-Newania, India; 18- Borden, Canada; 19-Phalaborwa, South Africa; 20-Chernigovka, Ukraine; 21- Hogenakkal, India; 22-Silinjarvi, Finland. The age estimates of these carbonatite provinces and additional details are provided in Table A.1.

of concentrated HF and $HNO_3$ followed by a 1:1 mixture of concentrated HCl and $HNO_3$ as described in Banerjee et al. (2016). The carbonatite standard COQ-1 was dissolved using the same protocol followed for the dissolution of WR-carbonatite samples as described earlier. The external reproducibility of the data, calculated by performing repeat measurements of AGV-2 and COQ-1, was better than 5% for most of the major and minor elements. While the external reproducibility for Ca concentration measurements was better than 5% for AGV-2, it was ~11% for the COQ-1 carbonatite standard. A 10-ppb internal standard solution comprising Be, Cs, In, and Bi were introduced "online" along with the sample and standard solutions to correct for instrumental drift during the measurements.

For Sr isotope ratio measurements, samples were dissolved using the protocol described above. Strontium was separated from the matrix using a two-stage ion-exchange chromatographic procedure where Sr was eluted in 3 M HCl from a Bio-Rad AG50W X8 (100–200 mesh) resin. The purified Sr was loaded on a Ta filament using 0.7 M $H_3PO_4$ and $Ta_2O_5$ activator was added on the top of the sample. The procedural blank for Sr was <400 pg. Strontium isotopic measurements were carried out using a Thermo Scientific Triton Plus thermal ionization mass spectrometer (TIMS) at the CEaS, IISc. The measured values of $^{87}Sr/^{86}Sr$ were normalized to $^{86}Sr/^{88}Sr = 0.1194$ using an exponential fractionation law to correct for instrumental mass fractionation. The uncertainty in $^{87}Sr/^{86}Sr$ is less than 0.000010, representing $2\sigma$ of the mean. The NIST SRM-987 Sr isotopic-standard analysed during this study yielded $^{87}Sr/^{86}Sr = 0.710264 \pm 10$ (2SD, $n = 7$). The detailed protocol for the measurements of Sr isotopic compositions of rock samples is described in Banerjee et al. (2016) and Banerjee and Chakrabarti (2019).

For Ca isotope ratio measurements, the WR carbonatites were dissolved using the same protocol adopted for investigation of their elemental abundances, whereas for the calcite separates, aliquots of the solutions prepared for elemental analysis were used. Sample solutions with ~10 μg Ca were mixed with an optimized amount of $^{43}Ca$-$^{48}Ca$ double spike (DS) mixture. These sample-spike mixtures were equilibrated at ~80 °C for approximately 6–8 h and subsequently evaporated. Calcium was purified using ion exchange chromatography (AG50W X8, 200–400 mesh resin) in Teflon columns and eluted using 2.5 M HCl. Each sample was passed twice through the columns and approximately 2.5 μg of purified Ca was loaded on a degassed tantalum filament using 0.8 M $HNO_3$ and a $Ta_2O_5$ activator was added on the top of the sample. Degassed rhenium filaments were used as ionization filaments and the isotopic measurements were performed using a double-filament geometry using the same Thermo Scientific Triton Plus TIMS at the CEaS, IISc cited above for Sr isotope measurements. The DS-TIMS technique used here for Ca isotopic measurements corrects for both instrumental mass-fractionation as well as possible fractionation during ion-exchange chromatography, which is an advantage over MC-ICPMS measurements employing solely sample-standard bracketing for correcting mass-fractionation. Additionally, the DS-TIMS technique for measuring Ca isotopes does not suffer from the formation of doubly-charged species, which is a clear advantage over MC-ICPMS measurements, particularly for analyses of Sr-rich carbonatites. The analytical details for Ca isotopic

measurements are described in Mondal and Chakrabarti (2018) and Banerjee and Chakrabarti (2019). The $\delta^{44/40}$Ca and $\delta^{44/42}$Ca values are reported relative to the NIST SRM 915a standard and the long-term external reproducibility of $\delta^{44/40}$Ca and $\delta^{44/42}$Ca, based on repeat measurements of standards, are better than 0.08‰ and 0.15‰ (2 SD), respectively.

To ascertain the relative proportions of Ca and Sr (and their corresponding Ca and Sr isotope compositions) present in the carbonate phases versus that of the whole rock (WR)- carbonatites, leaching experiments were performed on selected WR-carbonatite samples ($n = 10$) for which significant amount of sample was abundant. Approximately 500 mg of powdered WR-carbonatite samples were kept in 15 ml screwcap, flat-based Savillex© Teflon vials. For chemical extraction of carbonates from the powdered carbonatite samples, 10 ml of 10% acetic acid (v/v) was added to all the samples and ultrasonicated for 10 min for a complete homogenization. Acetic acid was used instead of HCl as it selectively leaches carbonates without affecting oxide and phosphate phases in carbonatites. After ultrasonication, all the vials were kept on a hot plate at a constant temperature of 60 °C. This chemical extraction method was carefully monitored, and all the vials were ultrasonicated further every fourth hour for a duration of 10 min. Chemical extraction of carbonates was continued until the fizzing of the samples completely stopped, which took about 15–18 h. Once fizzing stopped, vials were taken off the hot plate and ultrasonicated further. Subsequently, the whole mixture was carefully transferred to pre-cleaned 15 ml centrifuge tubes and centrifuged for 15 min at 3400 rpm. Once the centrifugation was complete, the supernatant fluid from each tube was carefully decanted to pre-cleaned Teflon vials without stirring the residue. This procedure of centrifugation for all the samples was conducted two more times with 18.2 MΩ-cm water, and each time the supernatant fluid was transferred to the respective Teflon vials. Upon decanting the supernatant fluid for the third time, the remaining residues from each centrifuge tube were transferred to a different set of pre-cleaned Teflon vials using 18.2 MΩ-cm water. Care was taken to minimize the sample loss when transferring the residues to Teflon vials. Vials containing residues and 18.2 MΩ-cm water as well as vials containing the supernatant solutions were kept on hot plate for drying and the dried residues were subsequently weighed. The proportion of the acid leached carbonate phase in each sample was calculated by subtracting the weight of the residue (non-carbonate phases) from the initial weight of the powdered carbonatite sample. All the dried carbonate fractions were stored with 10 ml of 2% (v/v) $HNO_3$ and HCl acid mixture.

For the determination of major and trace element concentrations for the carbonate fractions, an aliquot of 1 ml of acid mixture was taken in a pre-cleaned and pre-weighed 7 ml Teflon vial and kept on hot plate for drying. After this step, the vials with dried carbonate fractions were weighed again to estimate the weight of carbonate fractions for each sample. Subsequently, 2 ml of 2% nitric acid (v/v) were added to each of them for transferring to 125 ml pre-cleaned HDPE bottles (Tarsons, India). All the samples were diluted further by adding 2% nitric acid mixture to maintain a dilution factor of 4000 and 10,000 for the determination of trace and major element concentrations, respectively. Major and selected trace element concentrations and radiogenic Sr and stable Ca isotope ratios of only the carbonate fractions were measured using the same protocol followed for WR-carbonatite samples as explained earlier.

## 3. RESULTS

Major and trace element concentrations of the carbonatite samples (twenty-three WR carbonatites and seventeen calcite separates) and USGS rock standards, which were measured repeatedly during the analysis of the carbonatite samples, are reported in Table 1. Compositions of six WR-carbonatite samples from the Ambadongar Province, India, (Banerjee and Chakrabarti, 2019), are also reported in Table 1 together with the sole Ambadongar carbonatite sample (AMD003) analysed in this study.

Chemical classification of WR carbonatites, based on the ternary plot of MgO-CaO-MnO + $Fe_2O_{3(T)}$ (Woolley, 1982), suggests that among twenty-nine whole rock samples examined in this study, eighteen samples are calicocarbonatites, eight samples are ferrocarbonatites, and three samples are magnesiocarbonatites (Table 1 and Fig. 2). The major element compositions of the 17 calcites separates show significant compositional variability (Table 1). The K/Ca ratios for all the samples are extremely low, and the overall range is 0.000019–0.096 (Table 1). The Rb and Sr concentrations of the WR- carbonatites range from 0.054 to 65.78 ppm and 162.1 to 11280 ppm, respectively, while those for the calcite separates range from 0.34 to 35.33 ppm and 3924–85750 ppm, respectively (Table 1). The overall Rb/Sr ratios for calcite separates and WR carbonatite samples are low but define a large range (0.0000014–0.03; Table 1). The WR carbonatites show high rare earth element (REE) concentrations with light-REE (LREE) enrichments characteristic of carbonatites (Table 1, Fig. A.2).

Stable Ca isotopic compositions and $^{87}Sr/^{86}Sr$ values for the WR carbonatites and calcite separates investigated in this study are reported in Table 2. The Ca isotopic compositions of multiple Ca isotope standards (NIST SRM 915a, SRM 915b carbonates and NASS-6 seawater) and USGS rock standards (BCR-2, BHVO-2, AGV-2, DTS-2B and COQ-1), analysed during this study, are also reported in Table 2. Carbonatite samples show significant variations in $\delta^{44/40}Ca_{SRM915a}$ values ranging from 0.42 to 1.24‰ (Table 2, Fig. 3). Even for samples collected from the same geographic location, a broad range in $\delta^{44/40}Ca_{SRM915a}$ values is observed (Table 2, Fig. 4). For example, $\delta^{44/40}Ca_{SRM915a}$ values for samples from the ~120–130 Ma old Oka carbonatite complex of Canada range from 0.42 to 1.24‰ ($n = 8$), those from the South Indian Carbonatite complex (~800 Ma old Sevattur, Onnakarai, Garigapalli and ~2415 Ma old Hogenakkal) range from 0.65 to 0.91‰ ($n = 4$), those from the ~2060 Ma old Phalaborwa complex of South Africa range from 0.42 to 0.84‰ ($n = 3$), those from the ~65 Ma old Ambadongar complex

Table 1
Concentrations of selected major and trace elements of whole rock (WR) carbonatites and calcite separates from carbonatites analysed in the present study along with the compositions of acetic acid leached (L) carbonate fractions of selected WR carbonatite samples. Ages of these samples are also shown. Estimated carbonate fraction (%) in the leached carbonatite samples are shown within parenthesis. Also reported are the geochemical compositions of USGS standards analysed during this study. *Data for selected samples from Ambadongar are taken from Banerjee and Chakrabarti, 2019. CC: calciocarbonatites, FC: ferrocarbonatite, MC: magnesiocarbonatites.

| Sample# | Kalyango | Pollino | Vallone Toppo | K6 | K7 | 13–2 | AD L6(4)* | AD L7* | AD L7L | AD L11* | AD L11L | AD L13(1)* | AD L13(2)* | AD L24* | AMD003 |
|---|---|---|---|---|---|---|---|---|---|---|---|---|---|---|---|
| Location | Uganda | Umbria, Italy | Mt.Vulture, Italy | Kaiserstuhl, Badberg | Sukulu, Uganda | Ambadongar, India | | | | | | | | | |
| *Sample type* | *WR (FC)* | *WR (MC)* | *WR (CC)* | *WR (CC)* | *WR (CC)* | *Calcite* | *WR (CC)* | *WR (CC)* | *Leached (95%)* | *WR (FC)* | *Leached (76%)* | *WR (CC)* | *WR (CC)* | *WR (FC)* | *Calcite* |
| Age (Ma) | 0 | 0.246 | 0.75 | 16 | | 40 | 65 | | | | | | | | |
| Na (wt%) | 0.179 | 0.044 | 0.21 | 0.0112 | 0.093 | 0.025 | 0.027 | 0.0163 | | 0.020 | | 0.048 | 0.028 | 0.176 | 1.53 |
| Mg (wt%) | 4.4 | 5.2 | 1.47 | 0.105 | 2.4 | 1.10 | 0.090 | 0.21 | | 0.099 | | 0.26 | 0.061 | 0.94 | 0.22 |
| K (wt%) | 0.101 | 0.33 | 0.086 | 0.0065 | 0.031 | 0.0149 | 0.0091 | 0.0153 | | 0.0087 | | 0.61 | 0.0082 | 1.29 | 1.69 |
| Ca (wt%) | 25 | 23 | 28 | 46 | 37 | 42 | 18.3 | 56 | 32 | 26 | 30 | 27 | 39 | 13.4 | 28 |
| Fe (wt%) | 9.6 | 3.2 | 3.6 | 0.48 | 4.4 | 0.46 | 1.58 | 0.30 | | 7.0 | | 2.9 | 0.52 | 3.9 | 0.87 |
| Mn (wt%) | 0.37 | 0.049 | 0.32 | 0.092 | 0.50 | 0.153 | 0.094 | 0.167 | | 0.44 | | 0.35 | 0.130 | 0.31 | 0.191 |
| K/Ca | 4e-3 | 1.5e-2 | 3.1e-3 | 1.4e-4 | 8.4e-4 | 3.5e-4 | 5e-4 | 2.7e-4 | | 3.3e-4 | | 2.3e-2 | 2.1e-2 | 9.6e-2 | 5.9e-2 |
| Rb (ppm) | 4.4 | 49 | 12.9 | 0.51 | 1.99 | 0.44 | 7.0 | 0.49 | | 2.2 | | 53 | 0.27 | 66 | 35 |
| Sr (ppm) | 5325 | 1867 | 9211 | 10,140 | 7710 | 3924 | 2542 | 5417 | 4175 | 1700 | 1985 | 3483 | 2336 | 2098 | 6247 |
| La (ppm) | 825 | 146 | 626 | 325 | 1000 | | 596 | 448 | | 2630 | | 4153 | 985 | 1419 | |
| Ce (ppm) | 1549 | 321 | 1048 | 390 | 2464 | | 1083 | 779 | | 4741 | | 4800 | 1371 | 2020 | |
| Pr (ppm) | 168 | 27.6 | 103 | 21.7 | 217 | | 110 | 76.5 | | 494 | | 371 | 115 | 182 | |
| Nd (ppm) | 558 | 108 | 324 | 59 | 655 | | 335 | 163 | | 1484 | | 916 | 297 | 512 | |
| Sm (ppm) | 53 | 19.7 | 31.4 | 6.8 | 62 | | 43.6 | 22 | | 171 | | 97 | 30.9 | 67 | |
| Eu (ppm) | 13.9 | 4.08 | 8.3 | 2.38 | 16.7 | | 10.7 | 5.7 | | 39.6 | | 25.0 | 7.7 | 16.8 | |
| Gd (ppm) | 32.9 | 9.7 | 23.4 | 6.7 | 45.8 | | 37.9 | 25.6 | | 139 | | 112 | 30.2 | 65 | |
| Tb (ppm) | 4.61 | 1.73 | 3.32 | 0.87 | 6.3 | | 3.90 | 2.20 | | 12 | | 9.9 | 2.44 | 6.8 | |
| Dy (ppm) | 15.6 | 6.7 | 12.8 | 3.75 | 24.4 | | 15.8 | 9.2 | | 33.8 | | 34.1 | 7.2 | 28.8 | |
| Ho (ppm) | 2.57 | 1.06 | 2.35 | 0.79 | 4.25 | | 2.76 | 1.69 | | 4.68 | | 5.6 | 1.28 | 5.2 | |
| Er (ppm) | 6.50 | 2.49 | 6.25 | 2.29 | 10.8 | | 6.7 | 4.09 | | 9.1 | | 12.4 | 3.22 | 12.4 | |
| Tm (ppm) | 0.69 | 0.270 | 0.79 | 0.331 | 1.30 | | 0.97 | 0.55 | | 0.97 | | 1.41 | 0.444 | 1.61 | |
| Yb (ppm) | 4.52 | 1.72 | 5.1 | 2.17 | 8.3 | | 6.7 | 3.44 | | 6.1 | | 7.8 | 2.67 | 9.7 | |
| Lu (ppm) | 0.62 | 0.229 | 0.69 | 0.309 | 1.11 | | 0.962 | 0.473 | | 0.81 | | 0.90 | 0.300 | 1.25 | |
| Rb/Sr | 8.3e-4 | 2.7e-2 | 1.4e-3 | 5e-5 | 2.6e-4 | 1.1e-4 | 2.8e-3 | 9e-5 | | 1.3e-3 | | 1.5e-2 | 1.1e-4 | 3.1e-2 | 5.7e-3 |

| **Sample#** | **BMR056** | **MC117** | **SV15** | **SV15L** | **SV11** | **SV11L** | **SV12** | **SV12L** | **SV18** | **Tan213** | **OKA11** | **OKA27** | **OKA4A** | **OKA109** | **OKA206** |
|---|---|---|---|---|---|---|---|---|---|---|---|---|---|---|---|
| Location | Barmer, India | Magnet Cove, USA | Sung Valley, India | | | | | | | Panda Hill, Tanzania | Oka, Canada | | | | |
| *Sample type* | *Calcite* | *Calcite* | *WR (CC)* | *Leached (95%)* | *WR (CC)* | *Leached (89%)* | *WR (CC)* | *Leached (96%)* | *WR (MC)* | *Calcite* | *WR (CC)* | *WR (FC)* | *Calcite* | *Calcite* | *Calcite* |
| Age (Ma) | 68.57 | 97 | 107 | | | | | | | 116 | 120–130 | | | | |
| Na (wt%) | 0.37 | 0.0142 | 0.038 | | 0.048 | | 0.032 | | 0.111 | 0.043 | 0.131 | 0.021 | 0.160 | 0.084 | 0.191 |
| Mg (wt%) | 1.26 | 0.074 | 1.99 | | 1.86 | | 1.12 | | 8.4 | 1.33 | 1.55 | 0.0114 | 0.56 | 0.48 | 0.58 |
| K (wt%) | 0.0031 | 0.00085 | 0.046 | | 0.077 | | 0.00156 | | 0.90 | 0.0072 | 0.194 | 0.0060 | 0.153 | 0.196 | 0.027 |
| Ca (wt%) | 26 | 44 | 38 | 29 | 37 | 29 | 38 | 29 | 23 | 43 | 36 | 41 | 40 | 40 | 40 |
| Fe (wt%) | 2.5 | 0.183 | 0.69 | | 0.57 | | 2.8 | | 6.5 | 0.79 | 2.5 | 0.027 | 1.72 | 1.28 | 1.09 |
| Mn (wt%) | 3.2 | 0.0169 | 0.111 | | 0.172 | | 0.099 | | 0.24 | 0.59 | 0.56 | 0.00100 | 0.27 | 0.88 | 0.24 |
| K/Ca | 1.2e-4 | 1.9e-5 | 1.2e-3 | | 2.1e-3 | | 4.1e-5 | | 3.9e-2 | 1.7e-4 | 5.5e-3 | 1e-4 | 3.8e-3 | 04.9e-3 | 6.6e-4 |
| Rb (ppm) | 0.118 | 0.31 | 0.55 | | 2.1 | | 0.067 | | 26 | 0.25 | 12.9 | 0.065 | 17.7 | 4.9 | 1.30 |
| Sr (ppm) | 85,750 | 5786 | 4400 | 3727 | 4778 | 4313 | 3710 | 3244 | 2630 | 12,850 | 10,310 | 874.1 | 15,000 | 19,990 | 15,790 |
| La (ppm) | | | 194 | | 191 | | 165 | | 175 | | 986 | | | | |
| Ce (ppm) | | | 414 | | 428 | | 345 | | 411 | | 2600 | | | | |
| Pr (ppm) | | | 53 | | 58 | | 43.3 | | 58 | | 196 | | | | |
| Nd (ppm) | | | 205 | | 222 | | 166 | | 232 | | 551 | | | | |

| | | | | | | | | | | | | | | | | | | | | |
|---|---|---|---|---|---|---|---|---|---|---|---|---|---|---|---|---|---|---|---|---|
| Sm (ppm) | | | | 34.6 | | 37.6 | | 27.5 | | 40.3 | | | 53 | | | | | | | |
| Eu (ppm) | | | | 9.4 | | 10.0 | | 7.5 | | 10.7 | | | 16.4 | | | | | | | |
| Gd (ppm) | | | | 19.1 | | 20.7 | | 15.2 | | 22.1 | | | 48.9 | | | | | | | |
| Tb (ppm) | | | | 3.69 | | 3.88 | | 2.99 | | 3.92 | | | 7.3 | | | | | | | |
| Dy (ppm) | | | | 15.1 | | 15.4 | | 12.5 | | 15.3 | | | 30.5 | | | | | | | |
| Ho (ppm) | | | | 2.48 | | 2.49 | | 2.06 | | 2.38 | | | 5.2 | | | | | | | |
| Er (ppm) | | | | 5.3 | | 5.3 | | 4.46 | | 4.84 | | | 12.1 | | | | | | | |
| Tm (ppm) | | | | 0.61 | | 0.59 | | 0.51 | | 0.51 | | | 1.33 | | | | | | | |
| Yb (ppm) | | | | 3.58 | | 3.54 | | 3.02 | | 2.95 | | | 7.5 | | | | | | | |
| Lu (ppm) | | | | 0.466 | | 0.457 | | 0.390 | | 0.374 | | | 0.95 | | | | | | | |
| Rb/Sr | 1.4e-6 | 5e-5 | | 1.3e-4 | | 4.4e-4 | | 2e-5 | | 9.8e-3 | 2e-5 | | 1.3e-3 | 7e-5 | 1.2e-3 | 2.5e-4 | 8e-5 | | | |

| **Sample#** | **OKA153** | **OKA4B** | **OKA203** | **Jac-1** | **Jac-2** | **Jac-2L** | **13–19** | **13–6** | **S2** | **O2** | **O2L** | **G1** | **G1L** | **13–1** |
|---|---|---|---|---|---|---|---|---|---|---|---|---|---|---|
| Location | | Oka, Canada | | Jacupiranga, Brazil | | | Kovdor, Russia | Iron Hill, Colorado | Sevattur, South India | Onnakarai South India | | Garigapalli South India | | Prairie Lake, Canada |
| *Sample type* | *Calcite* | *Calcite* | *Calcite* | *WR (CC)* | *WR (FC)* | *Leached (77%)* | *Calcite* | *Calcite* | *WR (CC)* | *WR (CC)* | *Leached (81%)* | *WR (MC)* | *Leached (75%)* | *Calcite* |
| Age (Ma) | 120–130 | 131 | | | 379 | 570 | | | 800 | | | 1164 | | |
| Na (wt%) | 0.101 | 0.0171 | 0.47 | 0.041 | 0.036 | | 0.65 | 0.072 | 0.036 | 0.44 | | 0.0039 | | 0.030 |
| Mg (wt%) | 2.2 | 0.037 | 1.98 | 0.78 | 2.7 | | 0.87 | 0.27 | 3.6 | 1.62 | | 7.4 | | 0.131 |
| K (wt%) | 0.118 | 0.00129 | 0.022 | 0.0042 | 0.128 | | 0.62 | 0.0034 | 0.0152 | 0.43 | | 0.0095 | | 0.035 |
| Ca (wt%) | 36 | 46 | 35 | 42 | 23 | 21 | 37 | 41 | 29 | 34 | 28 | 27 | 22 | 42 |
| Fe (wt%) | 2.8 | 0.24 | 5.0 | 0.41 | 21 | 3224 | 1.56 | 2.3 | 1.28 | 1.51 | | 0.86 | | 0.34 |
| Mn (wt%) | 0.51 | 0.091 | 0.71 | 0.054 | 0.22 | | 0.113 | 0.44 | 0.37 | 0.022 | | 0.0146 | | 0.079 |
| K/Ca | 3.2e-3 | 2.8e-5 | 6.5e-4 | 1e-4 | 5.5e-3 | | 1.7e-2 | 8.3e-5 | 5.2e-4 | 1.3e-2 | | 3.5e-4 | | 8.4e-4 |
| Rb (ppm) | 13.6 | 0.25 | 1.70 | 0.189 | 5.21 | | 13.9 | 0.55 | 0.054 | 4.6 | | 0.073 | | 2.3 |
| Sr (ppm) | 11,600 | 18,260 | 11,100 | 5147 | 2666 | 3224 | 7693 | 8919 | 8205 | 162.1 | 183.6 | 295.8 | 240.7 | 15,160 |
| La (ppm) | | | | 273 | 177 | | | | 467 | 18 | | 7 | | |
| Ce (ppm) | | | | 613 | 410 | | | | 904 | 37 | | 15 | | |
| Pr (ppm) | | | | 78 | 53 | | | | 102 | 6.0 | | 1.61 | | |
| Nd (ppm) | | | | 217 | 151 | | | | 279 | 23.9 | | 5.9 | | |
| Sm (ppm) | | | | 37.6 | 26.5 | | | | 49.3 | 4.69 | | 1.18 | | |
| Eu (ppm) | | | | 10.0 | 7.0 | | | | 12.3 | 1.2 | | 0.220 | | |
| Gd (ppm) | | | | 19.0 | 13.1 | | | | 48.0 | 3.90 | | 1.22 | | |
| Tb (ppm) | | | | 3.41 | 2.35 | | | | 4.95 | 0.450 | | 0.167 | | |
| Dy (ppm) | | | | 13.3 | 9.0 | | | | 21.7 | 2.23 | | 0.97 | | |
| Ho (ppm) | | | | 2.03 | 1.33 | | | | 3.70 | 0.430 | | 0.201 | | |
| Er (ppm) | | | | 4.33 | 2.79 | | | | 8.39 | 1.13 | | 0.55 | | |
| Tm (ppm) | | | | 0.406 | 0.253 | | | | 1.06 | 0.164 | | 0.081 | | |
| Yb (ppm) | | | | 2.54 | 1.60 | | | | 6.3 | 1.03 | | 0.52 | | |
| Lu (ppm) | | | | 0.320 | 0.199 | | | | 0.88 | 0.143 | | 0.078 | | |
| Rb/Sr | 1.2e-3 | 1e-5 | 1.5e-4 | 4e-5 | 1.9e-3 | | 1.8e-3 | 6e-5 | 1e-5 | 2.9e-2 | | 2.5e-4 | | 1.5e-4 |

| Sample | NEW1 | NEW1L | NEW3 | NEW3L | NEW6 | 13–29 | PLP22A | PLP22C | PLP23 | 13–27 | H1 | 13–11 | COQ-1 | AGV-2 |
|---|---|---|---|---|---|---|---|---|---|---|---|---|---|---|
| Location | Newania, India | | | | | Borden, Canada | Phalaborwa, South Africa | | | Chernigovka, Ukraine | Hogenakkal, South India | Silinjarvi, Finland | Oka complex | Guano Valley |
| *Sample type* | *WR (FC)* | *Leached (89%)* | *WR (FC)* | *Leached (64%)* | *WR (FC)* | *Calcite* | *WR (FC)* | *WR (CC)* | *WR (CC)* | *Calcite* | *WR (CC)* | *Calcite* | *Carbonatite, USGS standard* | *Andesite, USGS standard* |
| Age (Ma) | | | 1473 | | | 1882 | | 2060 | | 2090 | 2415 | 2610 | | |
| Na (wt%) | | | | | | 0.0129 | 0.0066 | 0.034 | 0.043 | 0.039 | 0.132 | 0.0096 | 0.05 | 3.15 |
| Mg (wt%) | 8.1 | | 7.4 | | 9.2 | 1.03 | 3.0 | 3.6 | 5.7 | 0.81 | 1.26 | 2.2 | 0.76 | 1.06 |
| K (wt%) | 0.0075 | | 0.0151 | | 0.00091 | | 0.0190 | 0.0113 | 0.036 | 0.0022 | 0.181 | bdl | 0.171 | 2.48 |
| Ca (wt%) | 22 | 15 | 20 | 13 | 4 | 40 | 14.3 | 41 | 36 | 41 | 37 | 41 | 37 | 3.72 |
| Fe (wt%) | 9.2 | | 9.9 | | 24 | 0.82 | 41 | 0.89 | 2.0 | 0.88 | 0.44 | 0.92 | 2.27 | 4.70 |
| Mn (wt%) | 0.55 | | 0.59 | | 1.01 | 0.187 | 0.113 | 0.049 | 0.151 | 0.21 | 0.039 | 0.144 | 3607 | 770 |
| K/Ca | 3.5e-4 | | 7.5e-4 | | 2.3e-4 | | 1.3e-3 | 2.7e-4 | 9.9e-4 | 5.4e-5 | 4.9e-3 | | | |

| | | | | | | | | | | | | | | |
|---|---|---|---|---|---|---|---|---|---|---|---|---|---|---|
| Rb (ppm) | 1.15 | 1.17 | | 2.5 | 0.034 | 0.98 | 0.70 | 1.70 | 0.088 | 13.9 | 0.059 | 15.2 | | 70 |
| Sr (ppm) | 8637 | 6926 | 8089 | 1825 | 4691 | 2824 | 5181 | 11,280 | 7769 | 8531 | 9150 | 12,218 | | 655 |
| La (ppm) | 55 | 70 | | 99 | | 1228 | 515 | 968 | | 1253 | | | | |
| Ce (ppm) | 128 | 129 | | 282 | | 2349 | 1261 | 1941 | | 3312 | | | | |
| Pr (ppm) | 14.6 | 12.9 | | 33.6 | | 269 | 179 | 241 | | 304 | | | | |
| Nd (ppm) | 52 | 41.5 | | 132 | | 761 | 766 | 921 | | 1222.5 | | | | |
| Sm (ppm) | 8.0 | 5.4 | | 22 | | 73 | 97 | 104 | | 219 | | | | |
| Eu (ppm) | 2.25 | 1.46 | | 6.1 | | 8.5 | 15.5 | 20.2 | | 53 | | | | |
| Gd (ppm) | 6.6 | 4.69 | | 14.1 | | 25.4 | 39. 8 | 49.5 | | 161 | | | | |
| Tb (ppm) | 0.71 | 0.467 | | 1.69 | | 3.9 | 6.6 | 7.2 | | 16 | | | | |
| Dy (ppm) | 2.75 | 1.71 | | 5.8 | | 8.9 | 21.8 | 22 | | 64 | | | | |
| Ho (ppm) | 0.405 | 0.259 | | 0.75 | | 1.19 | 32 | 3.1 | | 8.8 | | | | |
| Er (ppm) | 0.88 | 0.62 | | 1.55 | | 2.0 | 7.08 | 7.4 | | 16 | | | | |
| Tm (ppm) | 0.083 | 0.058 | | 0.111 | | 0.201 | 0.57 | 0.59 | | 1.55 | | | | |
| Yb (ppm) | 0.440 | 0.331 | | 0.54 | | 1.23 | 3.9 | 4.1 | | 8.4 | | | | |
| Lu (ppm) | 0.056 | 0.0420 | | 0.064 | | 0.16 | 0.481 | 0.528 | | 1.08 | | | | |
| Rb/Sr | 1.3e-4 | 1.7e-4 | | 1.4e-3 | 1e-5 | 3.5e-4 | 1.3–4 | 1.5e-4 | 1e-5 | 1.6e-3 | 1e-5 | | | |

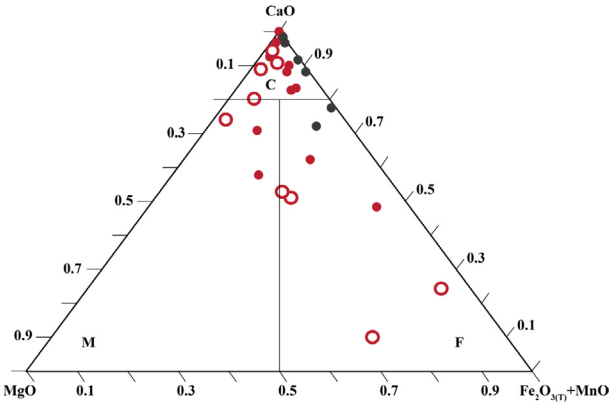


Fig. 2. A ternary plot of MgO-CaO-$Fe_2O_{3(T)}$ + MnO used for the classification of whole rock (WR) carbonatites (Woolley, 1982) showing the compositional domains of calcio (C)-, magnesio (M)- and ferro (F) -carbonatites. The compositions of the WR carbonatites analysed in this study (open and filled red circles representing older and younger carbonatites, respectively) are shown along with those from Ambadongar (filled black circles) reported by Banerjee and Chakrabarti (2019).

of India range from 0.53 to 1.05‰ ($n = 7$), those from the ~107 Ma old Sung Valley complex of India range from 0.65 to 0.74‰ ($n = 4$), those from the ~131 Ma Jacupiranga complex of Brazil range from 0.66 to 0.76‰ ($n = 2$), and those from the ~1473 Ma old Newania complex of India range from 0.81 to 0.90‰ ($n = 3$) (Table 2, Fig. 4). The measured $^{87}Sr/^{86}Sr$ for the carbonatites range from 0.70149 to 0.71044, while the initial $^{87}Sr/^{86}Sr$ ($^{87}Sr/^{86}Sr_{(t)}$) values range from 0.70149 to 0.71044 (Table 2, Fig. 5). It should be noted that due to the extremely low Rb/Sr of carbonatite samples, the measured and initial $^{87}Sr/^{86}Sr$ values are not very different. Significant variations in $^{87}Sr/^{86}Sr_{(t)}$ are also observed in carbonatite samples collected from the same geographical location (Table 2). For example, the $^{87}Sr/^{86}Sr_{(t)}$ values for carbonatites from the Oka complex range from 0.70332 to 0.70551, those from the south Indian carbonatite complex (ages 800 Ma and 2415 Ma) range from 0.70183 to 0.70808, those from the Phalaborwa complex range from 0.70415 to 0.70490, and those from the Ambadongar complex range from 0.70546 to 0.70623 (Table 2, Fig. 5).

Radiogenic Sr and stable Ca isotopic compositions of 10 leached carbonate phases from WR-carbonatite samples are reported in Table 2 while their Ca and Sr concentrations are reported in Table 1. The leaching experiments indicate that these carbonatites consist of 64–96 wt% carbonates as determined by comparing the weights of the initial powdered samples and those of the residues after the leaching experiments (Table 1). Stable Ca and radiogenic Sr isotope ratios for carbonates and corresponding WR samples show similar values within the analytical uncertainties, except sample O2 where the leachate yields higher $\delta^{44/40}Ca$ and less radiogenic $^{87}Sr/^{86}Sr$ (Table 2, Fig. A.3). Hence, only the WR data are used for further discussions.

Table 2
Stable Ca (w.r.t. NIST SRM915a) and radiogenic Sr isotopic compositions of whole rock (WR) carbonatites and calcites separated from carbonatites analysed in the present study along with the compositions of acetic acid leached (L) carbonate fractions of selected WR carbonatite samples. *Data for selected samples from Ambadongar are taken from Banerjee and Chakrabarti, 2019. Also reported are the stable Ca isotopic compositions of calcium isotope standards NIST SRM915a and SRM915b, modern seawater (NASS-6) and multiple USGS rock standards analysed during this study. CC: calciocarbonatites, FC: ferrocarbonatite, MC: magnesiocarbonatites.

| Sample | Location | Age (Ma) | Sample type | $\delta^{44/40}$Ca (‰) (w.r.t. NIST 915a) | 2SD | $\delta^{44/42}$Ca (‰) (w.r.t. NIST 915a) | 2SD | n | $^{87}Sr/^{86}Sr_{(0)}$ | $^{87}Sr/^{86}Sr_{(t)}$ |
|---|---|---|---|---|---|---|---|---|---|---|
| Kalyango | Uganda | 0 | WR (FC) | 0.62 | 0.07 | 0.31 | 0.10 | 2 | 0.704240 | 0.704240 |
| Pollino | Umbria, Italy | 0.246 | WR (MC) | 0.44 | 0.04 | 0.22 | 0.12 | 2 | 0.710444 | 0.710444 |
| Vallone Toppo | Mt.Vulture, Italy | 0.75 | WR (CC) | 0.89 | 0.04 | 0.42 | 0.14 | 2 | 0.706211 | 0.706211 |
| K6 | Kaiserstuhl, Badberg | 16 | WR (CC) | 0.85 | 0.06 | 0.4 | 0.14 | 2 | 0.703643 | 0.703643 |
| K7 | | | WR (CC) | 0.89 | 0.06 | 0.42 | 0.12 | 2 | 0.703659 | 0.703659 |
| 13–2 | Sukulu, Uganda | 40 | Calcite | 0.92 | 0.04 | 0.43 | 0.12 | 2 | 0.703127 | 0.703127 |
| ADL6(4)* | Ambadongar, India | 65 | WR (CC) | 0.85 | 0.06 | 0.43 | 0.14 | 2 | 0.705774 | 0.705767 |
| ADL7* | | | WR (CC) | 0.68 | 0.06 | 0.35 | 0.1 | 2 | 0.705462 | 0.705462 |
| ADL7L | | | Leached (95%) | 0.78 | 0.06 | 0.38 | 0.12 | 2 | 0.705466 | |
| ADL11* | | | WR (FC) | 1.05 | 0.03 | 0.47 | 0.14 | 2 | 0.705757 | 0.705754 |
| ADL11L | | | Leached (76%) | 1.02 | 0.04 | 0.47 | 0.1 | 2 | 0.705820 | |
| ADL13 (1)* | | | WR (CC) | 0.98 | 0.06 | 0.43 | 0.14 | 2 | 0.706287 | 0.706246 |
| ADL13(2)* | | | WR (CC) | 0.58 | 0.04 | 0.26 | 0.14 | 2 | 0.706232 | 0.706232 |
| ADL24* | | | WR (FC) | 1.05 | 0.04 | 0.46 | 0.1 | 2 | 0.706207 | 0.706123 |
| AMD003 | | | Calcite | 0.53 | 0.04 | 0.24 | 0.12 | 2 | 0.706040 | 0.706025 |
| BMR056 | Barmer, India | 68.57 | Calcite | 0.79 | 0.02 | 0.4 | 0.12 | 2 | 0.704339 | 0.704339 |
| MC117 | Magnet Cove, USA | 97 | Calcite | 0.92 | 0.02 | 0.45 | 0.10 | 2 | 0.703648 | 0.703648 |
| SV15 | Sung Valley, India | 107 | WR (CC) | 0.68 | 0.04 | 0.34 | 0.14 | 2 | 0.704862 | 0.704861 |
| SV15L | | | Leached (95%) | 0.73 | 0.04 | 0.37 | 0.1 | 3 | 0.704801 | |
| SV11 | | | WR (CC) | 0.71 | 0.06 | 0.36 | 0.14 | 2 | 0.704838 | 0.704836 |
| SV11L | | | Leached (89%) | 0.76 | 0.06 | 0.36 | 0.13 | 2 | 0.704802 | |
| SV12 | | | WR (CC) | 0.65 | 0.06 | 0.33 | 0.12 | 2 | 0.704812 | 0.704812 |
| SV12L | | | Leached (96%) | 0.75 | 0.04 | 0.34 | 0.12 | 2 | 0.704793 | |
| SV18 | | | WR (MC) | 0.74 | 0.06 | 0.35 | 0.14 | 2 | 0.704923 | 0.704880 |
| Tan213 | Panda Hill, Tanzania | 116 | Calcite | 0.85 | 0.08 | 0.41 | 0.12 | 2 | 0.703785 | 0.703785 |
| OKA11 | Oka, Canada | 120–130 | WR (CC) | 0.71 | 0.08 | 0.35 | 0.12 | 2 | 0.703327 | 0.703321 |
| OKA27 | | | WR (FC) | 0.42 | 0.06 | 0.21 | 0.12 | 2 | 0.705514 | 0.705514 |
| OKA4A | | | Calcite | 0.92 | 0.04 | 0.46 | 0.10 | 2 | 0.703321 | 0.703315 |
| OKA109 | | | Calcite | 0.90 | 0.07 | 0.41 | 0.12 | 2 | 0.703766 | 0.703765 |
| OKA206 | | | Calcite | 0.68 | 0.06 | 0.31 | 0.14 | 2 | 0.703843 | 0.703843 |
| OKA153 | | | Calcite | 0.56 | 0.06 | 0.26 | 0.12 | 2 | 0.703406 | 0.703400 |
| OKA4B | | | Calcite | 1.24 | | 0.57 | | 1 | 0.703355 | 0.703355 |
| OKA203 | | | Calcite | 0.85 | 0.06 | 0.39 | 0.14 | 2 | 0.703406 | 0.703405 |
| Jac-1 | Jacupiranga, Brazil | 131 | WR (CC) | 0.76 | 0.04 | 0.37 | 0.12 | 2 | 0.704868 | 0.704868 |
| Jac-2 | | | WR (FC) | 0.66 | 0.08 | 0.3 | 0.10 | 2 | 0.704851 | 0.704841 |
| Jac-2L | | | Leached (77%) | 0.70 | 0.07 | 0.35 | 0.1 | 3 | 0.704872 | |

| | | | | | | | | | | | |
|---|---|---|---|---|---|---|---|---|---|---|---|
| 13–19 | Kovdor, Russia | 379 | Calcite | 0.86 | 0.04 | 0.41 | 0.12 | 2 | 0.703557 | 0.703529 |
| 13–6 | Iron Hill, Colorado | 570 | Calcite | 0.83 | 0.06 | 0.39 | 0.12 | 2 | 0.703938 | 0.703937 |
| S2 | Sevattur (South India) | 800 | WR (CC) | 0.65 | 0.06 | 0.34 | 0.10 | 2 | 0.70537 | 0.705370 |
| O2 | Onnakarai (South India) | | WR (CC) | 0.66 | 0.08 | 0.31 | 0.12 | 2 | 0.708123 | 0.707180 |
| O2L | | | Leached (81%) | 0.8 | 0.08 | 0.4 | 0.12 | 3 | 0.707659 | |
| G1 | Garigapalli (South India) | | WR (MC) | 0.81 | 0.07 | 0.39 | 0.12 | 2 | 0.70809 | 0.708082 |
| G1L | | | LEached (75%) | 0.84 | 0.03 | 0.37 | 0.1 | 2 | 0.70807 | |
| 13–1 | Prairie Lake, Canada | 1164 | Calcite | 0.82 | 0.04 | 0.42 | 0.12 | 2 | 0.702593 | 0.702586 |
| NEW1 | Newania, India | 1473 | WR (FC) | 0.81 | 0.07 | 0.41 | 0.12 | 2 | 0.702055 | 0.702047 |
| NEW1L | | | Leached (89%) | 0.79 | 0.06 | 0.38 | 0.14 | 3 | 0.702066 | |
| NEW3 | | | WR (FC) | 0.88 | 0.04 | 0.41 | 0.10 | 2 | 0.702132 | 0.702122 |
| NEW3L | | | Leached (64%) | 0.84 | 0.06 | 0.39 | 0.12 | 3 | 0.702137 | |
| NEW6 | | | WR (FC) | 0.90 | 0.04 | 0.44 | 0.10 | 2 | 0.702148 | 0.702064 |

| Sample | Location | Age (Ma) | Sample type | $\delta^{44/40}$Ca (‰) (w.r.t. NIST 915a) | 2SD | $\delta^{44/42}$Ca (‰) (w.r.t. NIST 915a) | 2SD | n | $^{87}Sr/^{86}Sr_{(0)}$ | $^{87}Sr/^{86}Sr_{(t)}$ |
|---|---|---|---|---|---|---|---|---|---|---|
| 13–29 | Borden, Canada | 1882 | Calcite | 0.99 | 0.04 | 0.48 | 0.12 | 2 | 0.701827 | 0.701826 |
| PLP22A | Phalaborwa,South Africa | 2060 | WR (FC) | 0.42 | 0.06 | 0.18 | 0.12 | 2 | 0.704929 | 0.704899 |
| PLP22C | | | WR (CC) | 0.84 | 0.02 | 0.41 | 0.12 | 2 | 0.704166 | 0.704154 |
| PLP23 | | | WR (CC) | 0.71 | 0.02 | 0.35 | 0.14 | 2 | 0.704805 | 0.704792 |
| 13–27 | Chernigovka, Ukrain | 2090 | Calcite | 0.86 | 0.06 | 0.39 | 0.12 | 2 | 0.701925 | 0.701924 |
| H1 | Hogenakkal, South India | 2415 | WR (CC) | 0.91 | 0.08 | 0.45 | 0.10 | 2 | 0.701989 | 0.701825 |
| 13–11 | Silinjarvi, Finland | 2610 | Calcite | 0.85 | 0.06 | 0.41 | 0.12 | 2 | 0.701494 | 0.701493 |
| SRM915a | | | *standard - carbonate* | −0.02 | 0.05 | −0.02 | 0.10 | 4 | | |
| SRM915b | | | *standard - carbonate* | 0.74 | 0.06 | 0.38 | 0.14 | 2 | | |
| NASS-6 | | | *standard - seawater* | 1.86 | 0.04 | 0.92 | 0.12 | 4 | | |
| COQ-1 | Oka complex | | *USGS standard - carbonatite* | 0.69 | 0.06 | 0.33 | 0.10 | 3 | | |
| BCR-2 | Columbia River | | *USGS standard - basalt* | 0.8 | 0.06 | 0.41 | 0.12 | 2 | | |
| BHVO-2 | Hawaiian volcanic observatory | | *USGS standard - basalt* | 0.79 | 0.04 | 0.37 | 0.10 | 2 | | |
| AGV-2 | Guano Valley | | *USGS standard - andesite* | 0.77 | 0.08 | 0.36 | 0.14 | 2 | | |
| DTS-2B | Twin Sisters Mountain | | *USGS standard - dunite* | 1.29 | 0.08 | 0.61 | 0.14 | 2 | | |

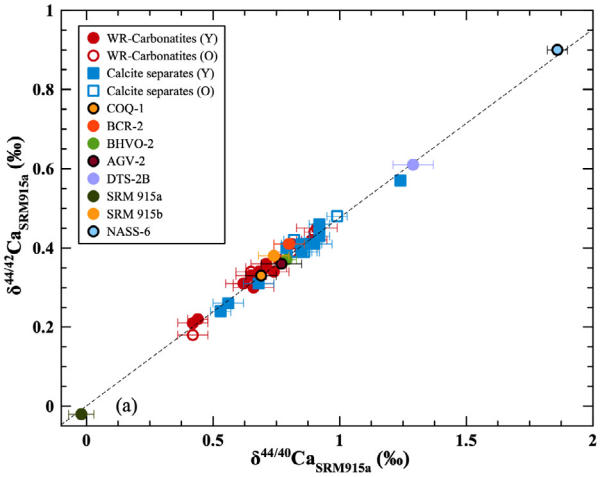


Fig. 3. Plot of $\delta^{44/42}$Ca versus $\delta^{44/40}$Ca (w.r.t. NIST SRM915a) showing compositions of globally distributed carbonatites from the present study. Also plotted are the stable Ca isotopic compositions of multiple Ca isotope standards (NIST SRM 915a, SRM 915b carbonates), modern seawater (NASS-6), and USGS rock standards (BCR-2, BHVO-2, AGV-2, DTS-2B and COQ-1) analysed during this study. All carbonatites plot on a mass-dependant fractionation line within their analytical uncertainties, thereby indicating that effect of radiogenic ingrowth of $^{40}$Ca on $\delta^{44/40}$Ca values is insignificant.

## 4. DISCUSSION

### 4.1. Sample dissolution and data accuracy

Use of hydrofluoric acid during the dissolution of rocks with high Ca concentrations could lead to the precipitation of calcium fluoride, which may potentially lead to stable Ca isotopic fractionation. In the present study, HF was sparingly used for the dissolution of the WR carbonatites as well the USGS carbonatite standard COQ-1 as described in Section 2. Formation of $CaF_2$ during sample dissolution can be tracked using rare earth element (REE) compositions as $CaF_2$ scavenges certain REEs and yields a 'W-type tetrad effect'; the latter results in an anomalous REE pattern for the supernatant solution (M−type tetrad effect) (e.g., Peretyazhko and Savina, 2010). Chondrite-normalized REE patterns for selected WR carbonatites from this study, dissolved using HF as described in Section 2, overlap with published REE patterns from the same provinces (Fig. A. 2). The REE compositions suggest that $CaF_2$ was not formed during dissolution of the WR carbonatites of this study, which rules out the role of $CaF_2$ formation in affecting the $\delta^{44/40}$Ca of these samples. Additionally, some of the WR carbonatites were leached with acetic acid and the Ca and Sr isotopic compositions of these leachates overlap with those of the WR samples dissolved using HF (Fig. A.3); the overlapping compositions rule out the formation of $CaF_2$ during dissolution of the WR carbonatites. Moreover, the accurate $\delta^{44/40}$Ca value obtained for the USGS carbonatite standard COQ-1 (Fig. A.4a), which was also dissolved using the same sample digestion protocol, validates both the analytical approach and Ca isotope results obtained in this study.

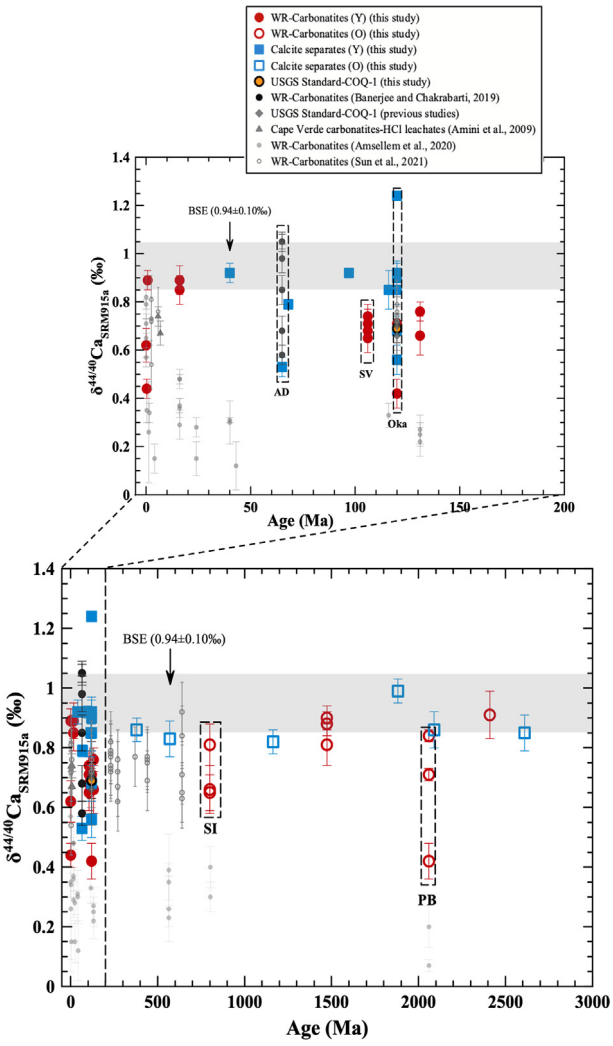


The Ca stable isotopic compositions of multiple Ca isotope standards (NIST SRM 915a, SRM 915b carbonates and NASS-6 seawater) and USGS rock standards (BCR-2, BHVO-2, AGV-2, DTS-2B and COQ-1) were determined during this study (Table 2). Our Ca isotope results for these standards, with widely different matrices, are consistent with their published isotope compositions (Feng et al., 2017; He et al., 2017; Kang et al., 2017; Li et al., 2018; Chen et al., 2019; Ionov et al., 2019; Liu et al., 2019; Sun et al., 2021). Specifically, our $\delta^{44/40}$Ca data for the USGS carbonatite standard COQ-1 overlaps with published Ca isotope measurements (Fig. A.4a.) (Feng et al., 2017; He et al., 2017, Li et al., 2018, Liu et al., 2019), which further validates the accuracy of the Ca isotope ratio measurements of this study performed using the double-spike TIMS measurement technique.

### 4.2. Effect of low-temperature alteration and $\delta^{44/40}$Ca of calcites versus whole-rock carbonatites

Since carbonatites consist predominantly of Ca-bearing minerals, they are consequently associated with extremely high concentrations of Ca, which would in turn buffer their

Fig. 4. Stable Ca isotopic compositions ($\delta^{44/40}$Ca w.r.t NIST SRM915a) of carbonatites analysed in this study (coloured symbols) from 22 occurrences worldwide versus their emplacement ages. These include 23 whole rock (WR) samples (open and filled red circles) and 17 calcites separated from carbonatites (open and filled blue squares) analysed in the present study along with the USGS carbonatite standard COQ-1 (filled orange circle with black edge). Also plotted are the compositions of six WR carbonatite samples from Ambadongar (AD) (Banerjee and Chakrabarti, 2019) (filled black circles) considered together with the data of this study. Additionally, data for leached carbonatite samples from the Cape Verde and the Canary Islands (filled grey triangle, Amini et al., 2009), globally distributed carbonatites from Amsellem et al. (2020) (grey filled circles) and Sun et al. (2021) ('primary carbonatites', grey open circles), the USGS carbonatite standard COQ-1 reported by other studies (filled grey diamond, Feng et al., 2017; He et al., 2017; Li et al., 2018; Liu et al., 2019) are also plotted. The horizonal shaded bar represents the estimated $\delta^{44/40}$Ca value of the bulk silicate Earth (BSE, 0.94 ± 0.10‰) (Kang et al., 2017; Chen et al., 2019). Although Kang et al. (2017) reported an external reproducibility of 0.05‰ (2SD) for the BSE value, we consider a conservative error bar of ±0.1‰ to reflect the reproducibility for $\delta^{44/40}$Ca measurements in most laboratories. Our data shows that most of the older (>300 Ma) carbonatites (O, open blue and red symbols), except those from the Neoproterozoic South Indian complex (SI) and Phalaborwa carbonatite complex (PB) of South Africa, show limited variation in $\delta^{44/40}$Ca values, which overlap with the $\delta^{44/40}$Ca of the BSE within their analytical uncertainties (2SD). Younger carbonatites (<300 Ma, both WR and calcite separates) (expanded in the inset; Y, filled red and blue symbols, respectively), which include multiple samples analysed from Oka ($n = 8$), Sung valley (SV) ($n = 4$) and Ambadongar (AD) complexes ($n = 7$; filled black circles), show a significant spread in the $\delta^{44/40}$Ca values with most samples showing $\delta^{44/40}$Ca values lower than that estimated for the BSE. See text for details.

Ca isotope compositions against post-emplacement, low temperature, surface alteration processes. Moreover, the majority of the carbonatite samples used in this study were previously studied for their $\delta^{13}$C and $\delta^{18}$O values and their compositions are suggestive of their pristine nature (Table A. 1). Hence, the $\delta^{44/40}$Ca values for these carbonatite samples reflect their pristine compositions and are not affected by post-emplacement low-temperature processes. The Ca and Sr isotopic data for both the WR carbonatites and calcite separates are considered together for further discussion since the WR aliquot is dominated by carbonate minerals, which control the Ca and Sr budgets of the WR sample. This feature has been previously demonstrated for the $^{87}Sr/^{86}Sr$ compositions of carbonate phases and their corresponding WR compositions (e.g., Castorina et al., 2000; Bizimis et al., 2003; D'Orazio et al., 2007; Wu et al., 2011). Additionally, overlapping values of $\delta^{44/40}$Ca and $^{87}Sr/^{86}Sr$ for the WR- carbonatites and their acid-leached carbonate phases further validate this assumption (Fig. A.3).

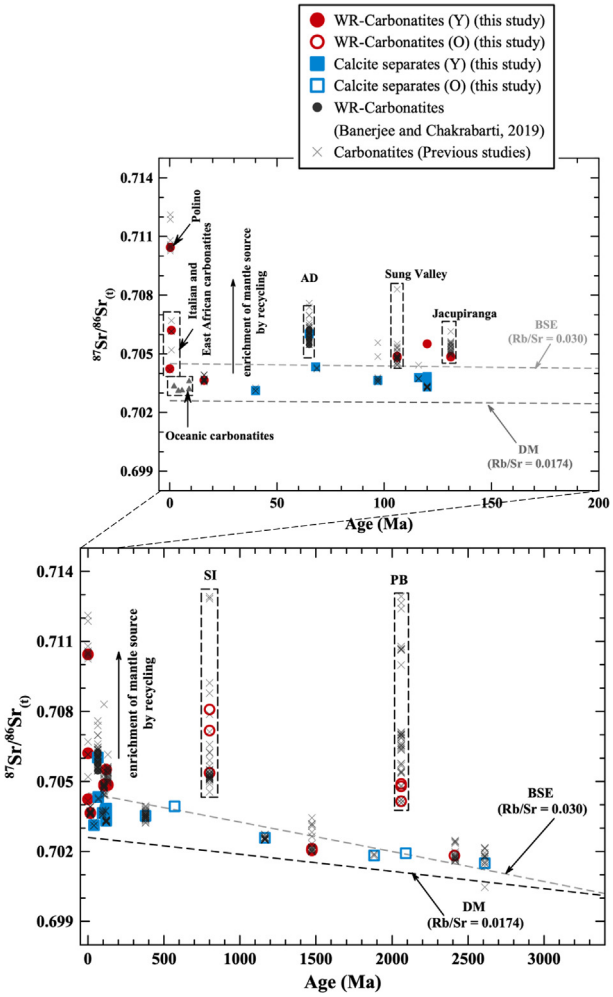


Fig. 5. Initial $^{87}Sr/^{86}Sr$ of global carbonatites (WR-carbonatites and calcite separates) analysed in this study (symbols same as Fig. 4) plotted versus their emplacement ages. Also plotted are published data (see Table A.1 for details) for carbonatites from the same geographical locations (grey crosses) as in this study. The black dashed line represents the Sr isotopic evolution curve of the depleted mantle (DM) with Rb/Sr = 0.0174 (Salters and Stracke, 2004) while the grey dashed line reflects the Sr isotopic evolution curve of the bulk silicate Earth (BSE) with Rb/Sr = 0.030 (McDonough and Sun, 1995). Older (>300 Ma) carbonatites, with low $^{87}Sr/^{86}Sr_{(t)}$, plot along an evolution line with Rb/Sr values intermediate between DM and BSE, except for samples from the Neoproterozoic South Indian carbonatite complex (SI) and Phalaborwa complex (PB) of South Africa (marked by dashed rectangles). In contrast, younger (<300 Ma) carbonatites show a large spread in $^{87}Sr/^{86}Sr_{(t)}$ with more radiogenic values indicating contribution from a mantle source enriched by crustal recycling. The $^{87}Sr/^{86}Sr$ of younger carbonatites are expanded in the inset, where published data for oceanic carbonatites are also plotted (filled grey triangles, Hoernle et al., 2002; Doucelance et al., 2010). Most of the younger carbonatite samples worldwide show radiogenic $^{87}Sr/^{86}Sr$ compared to the depleted mantle source compositions. See text for details.

### 4.3. Effect of radiogenic $^{40}$Ca on $\delta^{44/40}$Ca values

Since $^{40}$Ca is also produced by radioactive decay of $^{40}$K with a half-life of $1.277 \times 10^9$ years (Fantle and Tipper, 2014), radiogenic ingrowth of $^{40}$Ca can affect the measured $\delta^{44/40}$Ca values of rocks and minerals. This effect is quite significant for relatively old (>1 Ga) rocks and minerals with high K/Ca (>1) (Farkaš et al., 2011; Fantle and Tipper, 2014). Although relatively young rocks and minerals (<100 Ma old) with K/Ca < 2.5 typically do not show any significant contribution of radiogenic $^{40}$Ca on $\delta^{44/40}$Ca values (Fantle and Tipper, 2014), rocks and K-bearing minerals (e.g., phlogopite, K-feldspar, amphibole, clay minerals, etc.) of this age (<100 Ma) having K/Ca > 20 do indeed show significant contribution of radiogenic $^{40}$Ca on $\delta^{44/40}$Ca values (e.g., Farkaš et al., 2011; Fantle and Tipper, 2014; Banerjee and Chakrabarti, 2019). Older rocks with low K/Ca can still display significant enrichments in $^{40}$Ca despite losing their initial K during lower crustal metamorphic events (Antonelli et al., 2019), while younger rocks formed by partial melting of older rocks (>1 Ga) with high K/Ca could also inherit radiogenic $^{40}$Ca signatures (Mills et al., 2018). Therefore, it is important to assess whether there is any significant contribution of radiogenic $^{40}$Ca on the $\delta^{44/40}$Ca values for the carbonatite samples investigated here.

Typically, carbonatites are extremely enriched in Ca and depleted in K. The sole exceptions are the natrocarbonatites from the Oldoinyo Lengai in Tanzania (Jung et al., 2019), which have not been analysed in this study. Carbonatite samples analysed in the present study show K/Ca < 0.1 (Table 1). Therefore, it is unlikely that the $\delta^{44/40}$Ca values for the samples investigated here have been perturbed by contribution of radiogenic $^{40}$Ca. Moreover, in a plot of $\delta^{44/40}Ca_{SRM915a}$ versus $\delta^{44/42}Ca_{SRM915a}$ (Fig. 3), all the carbonatite samples plot on the theoretical mass-dependent fractionation line, which essentially rules out any effect of radiogenic $^{40}$Ca on the $\delta^{44/40}$Ca values for samples examined here. Hence, the large variation in $\delta^{44/40}$Ca values of the carbonatites investigated in this study either reflects their source mantle composition or different magmatic processes (e.g., crustal assimilation, diffusion, partial melting, and liquid immiscibility) and these possibilities are evaluated in the following sections.

### 4.4. Role of crustal assimilation and wall-rock interaction on $\delta^{44/40}$Ca of carbonatites

While pristine magmatic rocks typically show a limited range in $\delta^{44/40}$Ca values, crustal assimilation during ascent of the magma can introduce some variation in $\delta^{44/40}$Ca values (e.g., Mills et al., 2018; Banerjee and Chakrabarti, 2019). Under such circumstances, samples are expected to record the effect of radiogenic $^{40}$Ca ingrowth on the $\delta^{44/40}$Ca values, which, as discussed earlier, is not observed for the carbonatites investigated here. Average continental crust has an age of ~2.0 Ga and K/Ca < 1 (Antonelli et al., 2019). Assimilation of such old crust would alter the $\delta^{44/40}$Ca values of carbonatites by less than 0.1‰ (Fantle and Tipper, 2014), which is within the analytical uncertainties of $\delta^{44/40}$Ca measurements. Hence, crustal contamination, if it does occur, cannot explain the greater variation of the $\delta^{44/40}$Ca values (0.63‰) reported here. Moreover, carbonatites on average display ~10–20 times higher calcium concentration than average continental crust (Rudnick and Gao, 2004), which buffers the $\delta^{44/40}$Ca signatures of carbonatites against crustal assimilation. Finally, it is well-established that carbonatitic melts are characterized by low viscosity and density, which allows them to migrate through the continental crust rapidly without much interaction (e.g., Yaxley et al., 2020 and references therein).

An important mechanism of carbonatite melt evolution is melt-wall rock reaction (MRR) (Dasgupta et al., 2009; Chandra et al., 2019), which could result in diffusion-related kinetic isotope fractionations in the melts. Diffusion driven kinetic fractionation of stable Ca isotopes in mantle xenoliths has been advocated as a possible mechanism for lowering the $\delta^{44/40}$Ca values of mantle peridotites in multiple previous studies (Huang et al., 2010b; Zhao et al., 2017; Kang et al., 2020). Since the calcium concentration in carbonatite melts is much higher than surrounding silicate wall rocks, calcium would likely diffuse from the melt to the surrounding country rocks, with preferential and faster diffusion of the lighter isotopes relative to their heavier counterparts (e.g., Richter et al., 2008). Therefore, if MRR were to occur, this would result in progressively higher $\delta^{44/40}$Ca values in the carbonatite melts relative to their ambient mantle source. Such observation has been reported for some mantle xenoliths with $\delta^{44/40}Ca_{SRM915a}$ values as high as 3.3‰ (Kang et al., 2020). This hypothesis contrasts with the observed low $\delta^{44/40}$Ca values reported for some of the carbonatites of this study, and therefore suggests that diffusion-related isotopic fractionation cannot explain these low $\delta^{44/40}$Ca values.

### 4.5. Effect of partial melting of carbonated peridotites on the $\delta^{44/40}$Ca values of carbonatites

Partial melting and different degrees of melt extraction from residual mantle sources could result in small variations in $\delta^{44/40}$Ca values of the melt (Kang et al., 2017; Zhu et al., 2018, 2020b). This variation in $\delta^{44/40}$Ca values is expected to be observed if multiple samples from the same igneous complex are investigated. Model calculations suggest that silicate magmatic rocks formed by less than 25% partial melting of a spinel bearing peridotite- mantle source are unlikely to show variations in $\delta^{44/40}$Ca (e.g., Chen et al., 2019). In contrast, Wang et al. (2019a) suggested that silicate melts, generated by low degree partial melting of garnet- and jadeite- rich clinopyroxene-bearing peridotite mantle sources, show lower $\delta^{44/42}$Ca values (by ~0.14‰, which equates to ~0.29‰ in $\delta^{44/40}$Ca values assuming equilibrium isotope fractionation) than the peridotitic mantle source. The effect of partial melting on the $\delta^{44/40}$Ca of carbonatite melts has recently been evaluated (Sun et al., 2021). These authors argue that the lower $\delta^{44/40}$Ca values (relative to BSE) for 'primary' carbonatites, which have not been affected by hydrothermal alteration, is attributable to partial melting. A careful evaluation of the

partial melting model of Sun et al. (2021) reveals an error in the calculation of the $\Delta^{44/42}_{\text{garnet-melt}}$ parameter. Instead of calculating the $\Delta^{44/42}_{\text{garnet-melt}}$ values, the authors have determined the value(s) for $\Delta^{44/40}_{\text{garnet-melt}}$, although their results for $\Delta^{44/42}_{\text{cpx-melt}}$, $\Delta^{44/42}_{\text{opx-melt}}$, and $\Delta^{44/42}_{\text{ol-melt}}$ are correct. The incorrect calculation of $\Delta^{44/42}_{\text{garnet-melt}}$ has led to an overestimation of the Ca isotopic fractionation between the mantle source and the carbonatite melt. Using a model presented by Huang et al. (2019) and Zhang et al. (2018), we further evaluate the possible role of partial melting in generating the large range in $\delta^{44/40}$Ca values (0.63‰) for the carbonatites of the present study with $\delta^{44/40}Ca_{SRM915a}$ values as low as 0.42‰ (not considering Oka 4B which shows an anomalously high $\delta^{44/40}Ca_{SRM915a}$ value of 1.24‰).

For the model calculations, we consider a wide range of mantle depths (pressures, 3–10 GPa) and temperatures (1075–1500 °C) for the formation of carbonatite melts from the carbonated peridotite source, consistent with the estimation from multiple experimental petrology-based studies (e.g., Brey et al., 2008; Dasgupta and Hirschmann, 2006; Dasgupta et al., 2007, 2009). The major minerals in the source that may contribute towards the $\delta^{44/40}$Ca values of carbonatite melts are clinopyroxene and garnet, while the roles of orthopyroxene and olivine are insignificant but still considered for this model. The parameters used for the model calculations and results of the calculations are reported in the Table A.2.

The inter-mineral Ca isotopic fractionation has been calculated using the following formula:

$$\Delta^{44/40}Ca_{A-B} = 1000\,(\ln\beta_A - \ln\beta_B) \quad (1)$$

where A and B are two different co-existing minerals and 1000lnβ represents the reduced partition function ratios of $^{44}Ca/^{40}Ca$ which is defined by the following sets of equations:

$$1000\ln\beta = ax^3 + bx^2 + cx \quad (2)$$

$$\text{where, } x = 10^6/T^2 \text{ (T is the temperature in Kelvin)} \quad (3)$$

the values of coefficients a, b, and c are taken from Huang et al. (2019).

The Ca isotopic fractionation between clinopyroxene and the melt is expressed as

$$\Delta^{44/40}Ca_{CPx-melt} = 0.09/(T/1000)^2 \text{ (Zhang etal., 2018)} \quad (4)$$

while the other mineral-melt fractionation factors are expressed as

$$\Delta^{44/40}Ca_{Gt-melt} = \Delta^{44/40}Ca_{Gt-CPx} + \Delta^{44/40}Ca_{CPx-melt} \quad (5)$$

$$\Delta^{44/40}Ca_{OPx-melt} = \Delta^{44/40}Ca_{OPx-CPx} + \Delta^{44/40}Ca_{CPx-melt} \quad (6)$$

$$\Delta^{44/40}Ca_{Ol-melt} = \Delta^{44/40}Ca_{Ol-CPx} + \Delta^{44/40}Ca_{CPx-melt} \quad (7)$$

The results suggest that the variations in $\delta^{44/40}$Ca values in carbonatites due to partial melting of a (carbonated) peridotite ($\Delta^{44/40}Ca_{source-melt}$) would typically range from 0.05 to 0.15‰, for mantle melting temperatures ranging from 1075 to 1500 °C (Table A.2). In addition to temperature of melting, the $\Delta^{44/40}Ca_{source-melt}$ value also depends on the proportion of garnet and CPx in the source mantle (Table A.2). For mantle melting temperatures between 1400 and 1500 °C, the extent of Ca stable isotope fractionation between the mantle source and the carbonatite melts is typically less than 0.1‰, which is the analytical uncertainty associated with current $\delta^{44/40}$Ca measurements. However, if the source mantle has 20% garnet, the $\delta^{44/40}$Ca values of the carbonatite melt could be lowered by up to 0.12‰. At lower melting temperatures of 1075 °C, high amounts of garnet (10–15%) can result in lowering of $\delta^{44/40}$Ca values of the carbonatite melts by up to 0.15‰ (Table A.2). Overall, the extent of fractionation in $\delta^{44/40}$Ca values for carbonatite melts that may be attributable to partial melting of carbonated peridotite is significantly lower than the observed range in the $\delta^{44/40}$Ca values (0.63‰) for carbonatites of this study. Therefore, we suggest that partial melting has played a negligible role on the stable Ca isotopic compositions of carbonatite melts.

### 4.6. Effect of hydrothermal alteration on the $\delta^{44/40}$Ca values of carbonatites

Stable Ca isotopic compositions of carbonatites could be potentially modified from their pristine magmatic compositions if subjected to high temperature, post-emplacement/late-stage, hydrothermal alteration. Heated fluids can potentially dissolve Ca from the magmatic rocks and later precipitate Ca-bearing mineral phases. However, pervasive modification of Ca isotopic compositions of carbonatites due to late-stage hydrothermal processes is unlikely due to mass balance constraints. Fluorspar deposits associated with carbonatites from Ambadongar, India, are of hydrothermal origin and the high $\delta^{44/40}Ca_{SRM915a}$ of the fluorspar sample (1.44 ± 0.06‰) suggests that hydrothermal alteration can result in higher $\delta^{44/40}$Ca of carbonatites compared to the unaltered rock samples (Banerjee and Chakrabarti, 2019). In contrast, Sun et al. (2021) have suggested, based on a study of carbonatites from the Belaya Zima complex, Russia, that late-stage hydrothermal alteration could result in enrichment of both the light and heavy isotopes of Ca in 'non-primary' carbonatites; late-stage calcitic/dolomitic carbonatites show enrichment in the lighter isotopes while ankeritic carbonatites show enrichments in heavier isotopes of Ca. The authors argue that the changing composition of the hydrothermal fluid follows Rayleigh fractionation but do not provide any plausible evidence for the same. Additionally, the combined Ca and C isotopic compositions of some 'non-primary' carbonatites, considered to be affected by hydrothermal fluids, overlap with those of 'primary' carbonatites; these in turn show invariant Ca isotopic compositions similar to mantle-derived basalts, and are considered as pristine (Sun et al., 2021). These discrepancies highlight the complexities in delineating the role of hydrothermal alteration in modifying the Ca isotopic compositions of carbonatites. Out of the forty-six samples analysed in this study, one calcite sample from Oka (Oka 4B) shows an unusually high $\delta^{44/40}Ca_{SRM915a}$ value (1.24‰) compared to other samples from

this complex (Table 2). This sample may have been affected by late-stage hydrothermal alteration and is not considered for further discussion. However, given the complex, multi-stage evolutionary history of the Oka carbonatite complex (Chen and Simonetti, 2013, 2014), the exact cause for the high $\delta^{44/40}$Ca for sample Oka 4B cannot be ascertained.

### 4.7. Role of liquid immiscibility on $\delta^{44/40}$Ca of carbonatites

It has been postulated that carbonatites from several carbonatite complexes worldwide are petrogenetically associated with alkaline silicate rocks via liquid immiscibility involving a parental carbonated silicate melt (Jones et al., 2013 and references therein). Experimental petrology-based studies indicate that Ca is preferably partitioned into the carbonatite melts over the associated silicate melts (Freestone and Hamilton, 1980; Veksler et al., 1998, 2012), thereby leading to possible Ca isotopic fractionation during liquid immiscibility. However, the role of liquid immiscibility has not been explored by recent studies on the Ca isotopic compositions of carbonatites (Amsellem et al., 2020; Sun et al., 2021). During liquid immiscibility, the $\delta^{44/40}$Ca values of carbonatite and silicate melts, derived from a parent magma of mantle origin, would primarily depend on the Ca concentrations in the respective melts and proportions of carbonatite and silicate melts generated upon liquid immiscibility. Here we evaluate the effect of liquid immiscibility on the $\delta^{44/40}$Ca values of carbonatites using the following mass-balance equation:

$$\delta^{44/40}Ca_P = (\delta^{44/40}Ca_C * f_C * X_{Ca,C} + \delta^{44/40}Ca_S * f_S * X_{Ca,S}) / (f_C * X_{Ca,C} + f_S * X_{Ca,S}) \quad (8)$$

where $P$ represents the parent, mantle-derived, carbonated silicate magma prior to liquid immiscibility, while the subscripts C and S denote carbonatite and silicate melts, respectively. The mass fractions of carbonatite and silicate rocks present at a particular carbonatite complex are denoted by $f_C$ and $f_S$, respectively ($f_C + f_S = 1$), while $X_{Ca,C}$ and $X_{Ca,S}$ denote the fractions of Ca partitioned in the carbonatite and silicate melts, respectively, during liquid immiscibility ($X_{Ca,C} + X_{Ca,S} = 1$). For modelling purposes, the $\delta^{44/40}Ca_P$ is taken as 0.94‰, which is the estimated value of the BSE (relatively to SRM915a, Kang et al., 2017; Chen et al., 2019); while $f_C$ and $f_S$ are taken as 0.2 and 0.8, respectively, which are consistent with the relative proportions of carbonatites and alkaline silicate rocks present at the Ambadongar complex, India (Chandra et al., 2019). The value of $X_{Ca,C}$ has been varied from 0.7 to 0.9 (suggesting 70–90% of total Ca budget of parental magma being partitioned into the carbonatite melts upon liquid immiscibility), which is consistent with experimental estimates of Ca being mostly partitioned in the carbonatite melts compared to the conjugate silicate melts (Freestone and Hamilton, 1980; Veksler et al., 1998, 2012). The model results suggest that if liquid immiscibility is responsible for the low $\delta^{44/40}$Ca values in some carbonatites of this study ($\delta^{44/40}Ca_C$ value taken as 0.50‰), associated alkaline silicate rocks should have $\delta^{44/40}$Ca values (1.2–1.93‰) that are significantly higher than the estimated value for the BSE (0.94 ± 0.10‰) (Fig. 6). Such high

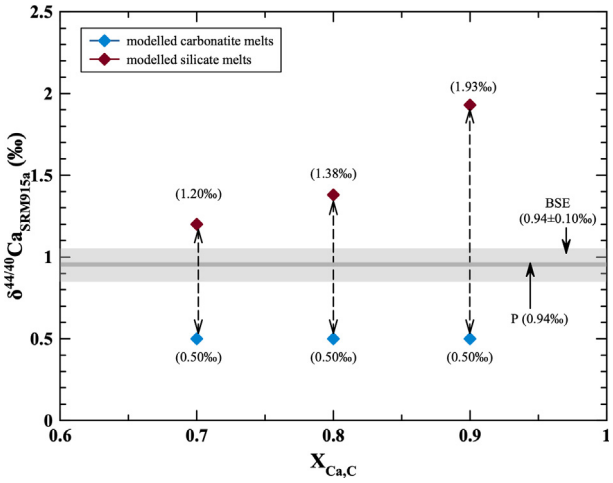


Fig. 6. Results of modelling calculations showing $\delta^{44/40}$Ca (w.r.t. NIST SRM 915a) of co-existing carbonatite and silicate melts versus fraction of Ca partitioned into the carbonatite melts ($X_{Ca,C}$) during liquid immiscibility. The thin horizontal dark grey bar (marked P) represents the parental melt ($\delta^{44/40}Ca_P$) with a $\delta^{44/40}$Ca value similar to the BSE (0.94‰) with a ±0.10‰ error bar (Kang et al., 2017; Chen et al., 2019; wide light grey horizontal bar). For carbonatite melts formed by liquid immiscibility and showing low $\delta^{44/40}$Ca like those observed in the present study (e.g., 0.50‰ considered in the model), the co-existing silicate melt will have unusually high $\delta^{44/40}$Ca, the value of which increases with increasing values of $X_{Ca,C}$. Such unusually high $\delta^{44/40}$Ca values have not been observed in alkaline silicate rocks which are often associated with carbonatites, thereby ruling out the role of liquid immiscibility in generating carbonatites with low $\delta^{44/40}$Ca. See text for details.

$\delta^{44/40}$Ca for silicate igneous rocks have not been reported. Additionally, the model predictions are not consistent with published Ca isotope data for the Ambadongar carbonatites and associated silicate igneous rocks (Banerjee and Chakrabarti, 2019). Increasing the $\delta^{44/40}Ca_C$ by 0.2‰ (i.e., 0.70‰) still results in $\delta^{44/40}$Ca values for associated silicate rocks that are higher than the BSE value, and contrast with observed $\delta^{44/40}$Ca values for silicate igneous rocks. Overall, the model results rule out the role of liquid immiscibility in generating carbonatites with low $\delta^{44/40}$Ca, as observed in some samples of this study. It may be noted that for carbonatites showing BSE-like $\delta^{44/40}$Ca, the role of liquid immiscibility on the Ca isotopic composition of carbonatites cannot be ascertained using a mass-balance model.

### 4.8. Temporal variation in $\delta^{44/40}$Ca of global carbonatites

The $\delta^{44/40}Ca_{SRM915a}$ values of the carbonatite samples examined in this study show significant variation of ~0.63‰ with a range of 0.42–1.05‰ (excluding Oka 4B which shows anomalously high $\delta^{44/40}Ca_{SRM915a}$, Table 2). However, as discussed above, processes such as partial melting, magma differentiation, diffusion, and liquid immiscibility fail to explain this variation. When plotted against their emplacement ages, it is evident that carbonatites with $\delta^{44/40}Ca_{SRM915a}$ values lower than BSE (0.94 ± 0.10‰;

Kang et al., Chen et al., 2019) are mostly younger than 300 Ma (Fig. 4). Out of the 29 pristine samples collected from 12 geographical locations with emplacement ages <300 Ma, 16 samples show $\delta^{44/40}$Ca values (including analytical uncertainties) lower than that of the BSE (Table 2, Fig. 4). In contrast, 12 out of 16 carbonatite samples collected from 10 different geographical locations with emplacement ages >300 Ma show BSE-like $\delta^{44/40}$Ca (Table 2, Fig. 4). Among these older carbonatites, two samples each from the Neoproterozoic South Indian and Phalaborwa complexes are characterized by low $\delta^{44/40}$Ca as discussed in detail in Section 4.10.

Our results contrast with a recently published Ca isotope dataset for globally distributed carbonatites, measured using multi-collector inductively coupled plasma mass spectrometry (MC-ICPMS) without using a double-spike technique, which reported $\delta^{44/40}$Ca values lower than BSE for all carbonatites irrespective of their emplacement age (Amsellem et al., 2020). The $\delta^{44/40}$Ca values reported by Amsellem et al. (2020), obtained by converting the measured $\delta^{42/44}$Ca to $\delta^{44/40}$Ca are significantly lower than the data presented in our study (Fig. 4) and those reported by Sun et al. (2021). Additionally, the $\delta^{44/40}$Ca values for carbonatite samples from oceanic settings (Cape Verde) reported by Amsellem et al. (2020) are significantly lower than those reported by Amini et al. (2009) (Fig. A.4b). While the $\delta^{44/40}$Ca for the BCR-2 standard (Columbia River Basalt) reported by Amsellem et al. (2020) overlaps with that reported in the present study, $\delta^{44/40}$Ca of carbonatites from Kaiserstuhl, Jacupiranga, Phalaborwa and the East African carbonatites as reported by Amsellem et al. (2020) are significantly lower than $\delta^{44/40}$Ca of carbonatites from the same locations reported here (Fig A.4b). The $\delta^{44/40}$Ca value of the USGS carbonatite standard COQ-1 analysed in this study matches with published results for this standard (Feng et al., 2017; He et al., 2017; Li et al., 2018; Liu et al., 2019) (Fig. A.4a); while Amsellem et al. (2020) have not reported Ca isotopic data for this carbonatite standard. Determining the exact reason for the discrepancy between the carbonatite dataset of Amsellem et al. (2020) and that of the present study is beyond the scope of this work.

Marine carbonates over time display a large range in $\delta^{44/40}$Ca values (Fig. A.1) (e.g., Farkaš et al., 2007a, b; Blättler et al., 2012; Fantle and Tipper, 2014; Blättler and Higgins, 2017). In contrast to the Precambrian carbonates, which show average $\delta^{44/40}$Ca values similar to the BSE (Blättler and Higgins, 2017), carbonates formed over the last 500 Ma show $\delta^{44/40}$Ca values lower than BSE (e.g., Farkaš et al., 2007a, b; Fantle and Tipper, 2014) (Fig. A. 1). Even in modern subduction zones, carbonate rich sediments are characterized by a large range of $\delta^{44/40}$Ca values (0.10–0.58‰), with an average value of 0.36‰, which are lower than that of the BSE (Zhu et al., 2020a). Therefore, introduction of recycled marine carbonates of Phanerozoic age, with low $\delta^{44/40}$Ca, into the mantle is expected to generate local Ca isotopic heterogeneities and will lower the $\delta^{44/40}$Ca of the mantle-derived melts affected by recycling. Low $\delta^{44/40}$Ca signatures linked to crustal carbonate recycling have been documented in Hawaiian basalts (Huang et al., 2011), calc-alkaline volcanics exposed in southeastern Tibetan Plateau (Liu et al., 2017) as well as carbonatites from Ambadongar, linked with the eruption of the Deccan Traps (Banerjee and Chakrabarti, 2019).

We argue that the low $\delta^{44/40}$Ca values of globally distributed carbonatites from this study with emplacement ages mainly younger than 300 Ma likely reflect mantle heterogeneity caused by increased carbonate recycling over the last few hundred million years. Recycling of marine carbonates with ages ranging from 100 to 200 Ma and 400–500 Ma (Fig. A.1a) can explain the $\delta^{44/40}$Ca of the younger carbonatites examined here and this is discussed in Section 4.9. This explanation is consistent with the high $\delta^{11}$B values of calcite separates from carbonatites younger than 300 Ma, which also suggests that incorporation of recycled crustal components in the mantle source of these rocks has been greater in recent geological times (e.g., Hulett et al., 2016; Cimen et al., 2018, 2019; Kuebler et al., 2020). Some of the calcite separates analysed by Hulett et al. (2016) were also analysed for $\delta^{44/40}$Ca in this study. Calcites from carbonatites older than 300 Ma display BSE-like values while few calcites from carbonatites younger than 300 Ma ($n = 4$) show lower $\delta^{44/40}$Ca consistent with the high $\delta^{11}$B observed in these samples (Fig. 7), both isotopic signatures indicative of crustal recycling. However, several calcites from young carbonatites (<300 Ma), which record high $\delta^{11}$B display BSE-like $\delta^{44/40}$Ca. The lack of a strong correlation between $\delta^{44/40}$Ca and $\delta^{11}$B values in the calcite separates from

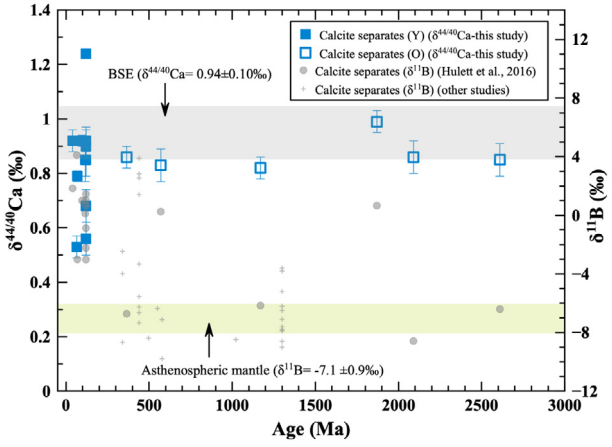


Fig. 7. Plot of $\delta^{44/40}$Ca (w.r.t. NIST SRM 915a) of calcite separates from carbonatites analysed in the present study (open and filled blue squares) and their corresponding $\delta^{11}$B values (filled grey circles, Hulett et al., 2016) versus the age of emplacement of the carbonatites. Also plotted are the $\delta^{11}$B of carbonatites from other locations (shown as grey cross-hairs, Cimen et al., 2018, 2019; Kuebler et al., 2020) which were not analysed for $\delta^{44/40}$Ca. The grey bar represents the $\delta^{44/40}$Ca value of the BSE (0.94‰) with a ±0.10‰ error bar (Kang et al., 2017; Chen et al., 2019) while the green coloured bar reflects the $\delta^{11}$B value of Earth's asthenospheric mantle ($\delta^{11}B = -7.1 \pm 0.9$‰) (Marschall et al., 2017). $\delta^{44/40}$Ca values lower than BSE are observed in some younger carbonatites (<300 Ma old) which also show high $\delta^{11}$B, both suggesting increased crustal recycling signatures in the younger carbonatites. See text for details.

carbonatites may be related to the different phases in which B and Ca are sequestered during crustal recycling. While the $\delta^{44/40}$Ca signature is most likely controlled by the recycling of marine carbonates, the $\delta^{11}$B signatures may reflect the fluxes of terrigenous and pelagic sediments (e.g., Kuebler et al., 2020).

Among the younger carbonatites, multiple samples were analysed from the ~65 Ma old Ambadongar, ~107 Ma old Sung Valley complexes of India, and the ~120–130 Ma old Oka complex of Canada. Samples from these complexes show clear trends towards lower $\delta^{44/40}$Ca values (Fig. 4). The low $\delta^{44/40}$Ca of the ~65 Ma old Ambadongar complex of India has been explained by the presence of ~160 million-year old recycled carbonates in the Réunion mantle plume source (Banerjee and Chakrabarti, 2019). The low $\delta^{44/40}$Ca for the carbonatites from the Sung Valley complex are consistent with their $\delta^{13}$C-$\delta^{18}$O and $\delta^{15}$N compositions, which suggest the presence of recycled ancient subducted oceanic carbonates in the Kerguelen mantle source region (Ray et al., 1999; Srivastava et al., 2005; Basu and Murty, 2015). Similarly, the broad range with low $\delta^{44/40}$Ca values of some carbonatites from the 120–130 Ma old Oka complex are consistent with the overall higher $\delta^{11}$B values of these samples, latter being interpreted as signature of recycled components in their mantle source (Hulett et al., 2016). Moreover, the median $\delta^{44/40}Ca_{SRM915a}$ value (0.71‰, $n = 7$, excluding sample Oka 4B with high $\delta^{44/40}$Ca) for the carbonatites from the Oka complex analysed in this study overlaps with the $\delta^{44/40}Ca_{SRM915a}$ value (0.69 ± 0.08‰) obtained for the COQ-1 USGS carbonatite standard from the same complex (Table 2), and published results for this standard (Fig. 4 and A.4a). To further evaluate the large spread in low $\delta^{44/40}$Ca values for carbonatites younger than 300 Ma, which contrasts to those for most of the older carbonatites, their corresponding radiogenic Sr isotopic signatures are considered since $^{87}$Sr/$^{86}$Sr is a powerful isotope tracer for delineating mantle source characteristics and is not affected by magmatic processes such as partial melting or fractional crystallization.

### 4.9. Sr isotopic variations in carbonatites and its covariation with $\delta^{44/40}$Ca in young carbonatites

The carbonatite samples examined in this study show a wide range in $^{87}$Sr/$^{86}Sr_{(t)}$ (Fig. 5). The lowest $^{87}$Sr/$^{86}Sr_{(t)}$ values for the carbonatites of a particular age plot along a single evolution line, which corresponds to a depleted mantle-like Rb/Sr ratio of 0.0174 (Salters and Stracke, 2004) (Fig. 5). This is also consistent with the estimated Rb/Sr ratio of the long-term depleted mantle source regions of carbonatites from different tectonic locations (Bell et al., 1982; Rukhlov et al., 2015), and different from the estimated Rb/Sr ratio of 0.030 for the bulk silicate Earth (BSE) (McDonough and Sun, 1995) (Fig. 5).

While the $^{87}$Sr/$^{86}Sr_{(t)}$ signatures for most of the older carbonatites (excluding Phalaborwa and south Indian carbonatites) are indicative of derivation from a depleted mantle source, those for carbonatites younger than 300 Ma define a large scatter with more radiogenic $^{87}$Sr/$^{86}Sr_{(t)}$ values. Some of these younger carbonatites are also characterized by lower $\delta^{44/40}$Ca values compared to the BSE as discussed earlier. The higher $^{87}$Sr/$^{86}Sr_{(t)}$ values may be attributed to crustal assimilation during ascent and emplacement, given the more radiogenic $^{87}$Sr/$^{86}$Sr of continental crust. However, for carbonatites, the effect of crustal contamination is expected to be minimal as Sr concentrations in carbonatites are 10 to 100 times higher than continental crustal rocks (e.g., Jones et al., 2013).

Therefore, we argue here that the Sr isotopic compositions for most of these carbonatites reflect those inherited from their mantle source, and any trend towards more radiogenic $^{87}$Sr/$^{86}$Sr compositions reflect enrichment due to incorporation of recycled oceanic lithosphere along with pelagic and/or terrigenous sediments into the mantle (Hofmann, 1997; Stracke et al., 2003, 2005; Workman et al., 2004; Willbold and Stracke, 2006, 2010; Bell and Simonetti, 2010). Hence, the most viable interpretation for explaining the more radiogenic $^{87}$Sr/$^{86}Sr_{(t)}$ compositions for the younger carbonatites is their derivation from mantle reservoir(s) with recycled components.

A negative trend is observed between $\delta^{44/40}$Ca and $^{87}$Sr/$^{86}Sr_{(t)}$ of carbonatite samples worldwide younger than 300 Ma (Fig. 8a), which suggests that crustal recycling has been more prominent during the last 300 million years; this is consistent with the B isotopic compositions of carbonatites on a global scale (Fig. 7) (Hulett et al., 2016, Kuebler et al., 2020). The co-variation of $\delta^{44/40}$Ca and $^{87}$Sr/$^{86}Sr_{(t)}$ for most of the younger carbonatites (excluding one carbonatite from Polino) can be explained by binary mixing between mantle peridotite/eclogite source and recycled carbonates of age 400–500 and/or 100–200 Ma. Our model calculation, which is based on $\delta^{44/40}$Ca and $^{87}$Sr/$^{86}Sr_{(t)}$ ratios for mantle peridotite and eclogite sources and marine carbonates of different ages (Table 3), suggests that the Ca and Sr isotopic compositions of majority of younger carbonatites (<300 Ma) examined here can be explained by the presence of less than 10 wt% of recycled crustal carbonates in their mantle sources (Fig. 8b).

Of note, Fig. 8b illustrates that the $^{87}$Sr/$^{86}Sr_{(t)}$ and $\delta^{44/40}$Ca of younger carbonatites are not perfectly correlated. One possible explanation is the fact that $\delta^{44/40}$Ca values and $^{87}$Sr/$^{86}$Sr of marine carbonates are controlled by different processes. The $^{87}$Sr/$^{86}$Sr ratios of marine carbonates mimic the seawater composition, and the latter in turn depends on the relative fluxes of continental- and mantle-derived Sr. In contrast, the $\delta^{44/40}$Ca values of marine carbonates do not have the same composition as seawater as stable Ca isotopes are fractionated during precipitation of carbonates. In addition to the compositions of source fluxes, the $\delta^{44/40}$Ca values of marine carbonates depend on the isotopic fractionation factor, which in turn depends on multiple factors such as seawater temperature, carbonate mineralogy, etc. Hence, while carbonate subduction reduces the $\delta^{44/40}$Ca values and increases the $^{87}$Sr/$^{86}$Sr of the mantle-derived melts influenced by this recycling process, these values may not show a 1:1 correlation, as observed in the younger carbonatites of the present study.

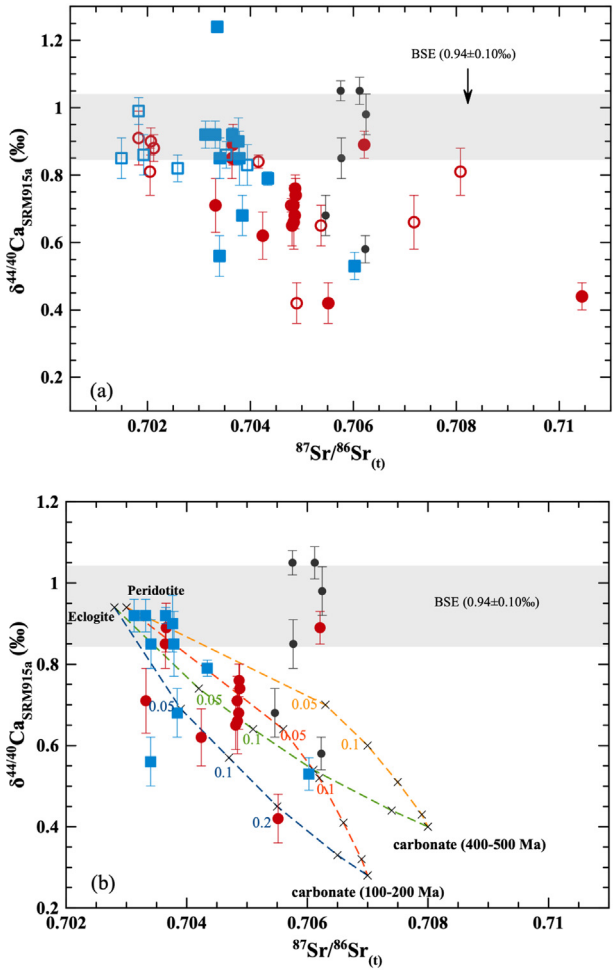


Fig. 8. **(a)** Plot of $\delta^{44/40}$Ca (w.r.t. NIST SRM 915a) versus $^{87}Sr/^{86}Sr_{(t)}$ of whole-rock carbonatites (open and filled red circles) and calcite separates from carbonatites (open and filled blue squares) analysed in the present study and those from Ambadongar (filled black circles, Banerjee and Chakrabarti, 2019). The horizontal bar represents the estimated $\delta^{44/40}$Ca of the BSE (0.94‰) with a ±0.10‰ error bar (Kang et al., 2017; Chen et al., 2019). The overall negative trend observed in the pristine carbonatites is explained by recycling of crustal carbonates of different ages. See text for details. **(b)** Plot of $\delta^{44/40}$Ca versus $^{87}Sr/^{86}Sr_{(t)}$ of pristine WR carbonatites (filled red circle) and calcite separates (filled blue squares) younger than 300 Ma showing model mixing curves between a peridotite and eclogitic mantle and crustal carbonates of two different ages (100–200 Ma and 400–500 Ma). Blue and red dashed curves represent mixing curves between100-200 Ma old carbonates and eclogitic and peridotitic mantle sources, respectively; green and orange curves represent mixing lines between 400–500 Ma old carbonates with eclogitic and peridotitic mantle sources, respectively. The $\delta^{44/40}$Ca of most of the younger carbonatites (<300 Ma) of this study can be explained by less than 10 wt% contribution of subducted carbonates; one sample from the Oka complex (Oka 27) requires contribution of ~20 wt% recycled carbonates. End member compositions used for modelling calculations are reported in Table 3.

Additionally, the lack of perfect correlation between $\delta^{44/40}$Ca values and $^{87}Sr/^{86}Sr$ of carbonatites may also arise from the fact that while the $\delta^{44/40}$Ca values are primarily controlled by subducted marine carbonates, $^{87}Sr/^{86}Sr$ could also be affected by the input of recycled terrigenous and pelagic sediments.

Table 3
End-member compositions used for generating model mixing curves shown in Fig. 8a. The four mixing curves represent mixing of the mantle peridotite/eclogite with subducted carbonates of ages 100–200 Ma and 400–500 Ma. The $\delta^{44/40}$Ca of carbonates are based on Fig. A1. Other end-member compositions are taken from (Chen et al., 2019; Doucelance et al., 2010; Huang et al., 2011; Salters and Stracke, 2004; Smart et al., 2021; Sun and McDonough, 1989; Veizer and Compston, 1976; Palme and O'Neill, 2014).

| End members | Ca (wt%) | $\delta^{44/40}$Ca (‰) | Sr (ppm) | $^{87}Sr/^{86}Sr_{(t)}$ |
|---|---|---|---|---|
| Mantle peridotite | 2.54 | 0.94 | 22 | 0.703 |
| Mantle Eclogite | 3.5 | 0.94 | 112 | 0.7028 |
| Carbonates (100–200 Ma) | 40 | 0.28 | 800 | 0.707 |
| Carbonates (400–500 Ma) | 40 | 0.4 | 800 | 0.708 |

Among the younger carbonatites, the solitary magnesiocarbonatite sample from Polino, Italy shows a unique composition. This carbonatite sample displays a low $\delta^{44/40}Ca_{SRM915a}$ value (0.44 ± 0.04‰), which suggests carbonate recycling in its mantle source, and its young eruption age precludes radiogenic ingrowth of $^{40}$Ca (Table 2). However, the extremely radiogenic $^{87}Sr/^{86}Sr$ of this sample (0.71044) cannot simply be explained by carbonate recycling and is not considered in the modelling calculations in Fig. 8b. The radiogenic $^{87}Sr/^{86}Sr$ of this carbonatite sample is consistent with the previously reported Sr isotopic ratios of carbonatites from this complex (e.g., Castorina et al., 2000; Bell et al., 2013). These earlier studies, focused on radiogenic isotope ratios of carbonatites from Polino, have explained the derivation of these carbonatites from a source defined by mixing between depleted mantle and a unique enriched mantle referred to as the Italian Enriched Mantle (ITEM; Bell et al., 2013).

### 4.10. Unique compositions of the Phalaborwa and South Indian carbonatites

As mentioned earlier, twelve out of sixteen carbonatite samples older than 300 Ma show BSE-like $\delta^{44/40}$Ca values. However, two carbonatite samples each from the Neoproterozoic carbonatite complex of South India and the 2060 Ma old Phalaborwa complex of South Africa display low $\delta^{44/40}$Ca values (Fig. 4, Table 2). These carbonatite samples also display more radiogenic $^{87}Sr/^{86}Sr_{(t)}$ compared to other carbonatites older than 300 Ma (Fig. 5, Table 2).

Based on the Nd, Sr and Os isotopic compositions, it has been suggested that carbonatites from the Sevattur complex (one of the Neoproterozoic south Indian carbonatite complexes of age 800 Ma) represent less than 10% recycled carbonates in their mantle source without any significant crustal assimilation; however, the parental carbonatite melts from the Samalpatti complex (another Neoproterozoic south Indian carbonatite complex of age 800 Ma) have long-preserved K-rich ancient crustal components, which is consistent with their high $\delta^{13}$C, $\delta^{18}$O, non-radiogenic Nd

isotopic compositions and relatively high $SiO_2$ (>20 wt%) (Kumar et al., 1998; Schleicher et al., 1998; Pandit et al., 2002; Ackerman et al., 2017, 2019). The low $\delta^{44/40}Ca_{SRM915a}$ (0.65 ± 0.06‰) and the $^{87}Sr/^{86}Sr_{(t)}$ (0.70573) of the 800 Ma old carbonatite sample S2 from Sevattur in South India are best explained by the recycling of old carbonates (e.g., ~1100 Ma old with average $\delta^{44/40}Ca_{SRM915a}$of 0.41‰) in their mantle source (see Fig A.1b). The 800 Ma old WR carbonatite sample O2 (Onnakarai, Samalpatti complex, South India) also shows low $\delta^{44/40}Ca_{SRM915a}$ (0.66 ± 0.08‰) and radiogenic $^{87}Sr/^{86}Sr_{(t)}$ (0.70718); while the low $\delta^{44/40}Ca$ value can be explained by carbonate recycling (e.g., ~1100 Ma old with average $\delta^{44/40}Ca_{SRM915a}$ of 0.41‰) (Fig. A.1b), the $^{87}Sr/^{86}Sr_{(t)}$ of these 800 Ma old carbonatites are more radiogenic than marine carbonates older than 800 Ma. The radiogenic $^{87}Sr/^{86}Sr$ of the Samalpatti carbonatite sample most likely reflects pre-emplacement interaction with the ambient crust, as suggested by Ackerman et al. (2017, 2019), which did not affect the Ca isotopic composition of the carbonatite melts due to their extremely high Ca concentrations.

Out of the three carbonatite samples analysed from Phalaborwa, South Africa, one calciocarbonatite sample displays BSE-like $\delta^{44/40}Ca_{SRM915a}$ value, a second calciocarbonatite shows a slightly lower $\delta^{44/40}Ca_{SRM915a}$ value (0.71 ± 0.02‰), while the third sample, a ferrocarbonatite, yields an even lower $\delta^{44/40}Ca_{SRM915a}$ value (0.42 ± 0.06‰) (Table 2). The Phalaborwa carbonatite complex hosts copper and zirconium metal deposits (Bell and Blenkinsop, 1989; Wu et al., 2011). However, the Ca and Sr isotopic compositions of these carbonatites are unlikely to be affected by the large-scale Cu and Zr mineralization, given the extremely high concentrations of Ca and Sr of carbonatites compared to the associated metal deposits. As demonstrated earlier, partial melting of mantle source, liquid immiscibility or diffusion-based kinetic isotopic fractionation are unlikely interpretations for the lower $\delta^{44/40}Ca$ of these two samples. Therefore, one possibility for the low $\delta^{44/40}Ca$ values of these carbonatites ($n = 2$) reflect their isotopically heterogeneous mantle source composition, which may be attributed to carbonate recycling associated with the subduction of Northern Oceanic plate due to closure of the Zimbabwe Craton to form the Kalahari Craton (Ernst and Bell, 2010). Although ~2.1 Ga or older carbonates show a significantly broad range in the $\delta^{44/40}Ca$ values, their average value are similar to BSE (Fig A.1b). However, if average $\delta^{44/40}Ca$ values are calculated at 100 Ma intervals, 2.4 Ga, 2.6 Ga, 2.8 Ga, and 3.0 Ga old carbonates show compositions lower than the estimated value of the BSE (Fig A.1b). Recycling of crustal carbonates of similar compositions could explain the low $\delta^{44/40}Ca$ of the Phalaborwa carbonatites. This interpretation is consistent with the presence of mass-independent fractionation (MIF) signatures of S isotopes in these carbonatites (Bolhar et al., 2020) which also suggest the presence of at least 2.45 Ga old recycled components in their mantle-source. In contrast to the $\delta^{44/40}Ca$ values of the Phalaborwa carbonatite samples, the radiogenic $^{87}Sr/^{86}Sr$ of these carbonatites cannot be explained by carbonate recycling due to the similar $^{87}Sr/^{86}Sr$ of the depleted mantle and marine carbonates prior to 2.06 Ga (Veizer, 1976). An earlier, detailed study, based on radiogenic Sr, Nd and Hf isotopic compositions of Phalaborwa carbonatites, postulated that these carbonatite melts could have formed from an enriched harzburgitic continetal lithospheric mantle source with heterogeneously distributed eclogitic components (Wu et al., 2011). However, the presence of eclogites in the mantle source of Phalaborwa complex is indeed a signature of the presence of recycled components in the mantle source of these rocks. Overall, crustal recycling signatures in some Proterozoic carbonatites is consistent with the onset of plate tectonics (e.g., El Dien et al., 2019, 2020), but these signatures were sporadic, which contrasts with the widespread signatures of crustal recycling in carbonatites younger than 300 Ma (Figs. 4, 5, 8).

### 4.11. Recent increase in crustal carbonate recycling and implications for mantle geodynamics

Based on global dynamic plate tectonic models that include plate rotations and digital age grids of the sea floor, it has been suggested that between ~180 and 130 Ma ago, a large amount of subducted material was recycled into the mantle due to a sharp increase in the convergence rate (East et al., 2020). Additionally, a plate motion model-based investigation has argued that the high flux of subducted material occurred thrice between 410 Ma and present day (Hounslow et al., 2018). These enhanced crustal recycling episodes could be due to changes in the geotectonic conditions of upper mantle possibly linked with the formation (Late Paleozoic) and subsequent break up (Late Jurassic) of Pangea (Collins, 2003, and references therein). Ernst and Bell (2010) argue that most carbonatites emplaced within the past ~250 million years are temporally and spatially linked with different large igneous provinces (LIP), which are primarily related to plume-related magmatism. Temporal distribution of large igneous provinces (LIP) suggest that the plume activity was much more pronounced during the past 250 million years (Ernst, 2014), thereby, delivering increased amounts of mantle material, much of which has been modified by recycling over time (Shaw et al., 2012). It is possible that the increased signatures of crustal carbonate recycling (low $\delta^{44/40}Ca$ and associated radiogenic $^{87}Sr/^{86}Sr$) in globally distributed carbonatites younger than 300 Ma are indicative of changes in the upper mantle geodynamics in the last 300 million years, specifically the increased recycling of crustal material and subsequent resurfacing by plume activity. A similar argument was put forward by Hulett et al. (2016) based on the $\delta^{11}B$ values for carbonatite occurrences worldwide. A compilation of $\delta^{44/40}Ca$ values of marine carbonates shows that the $\delta^{44/40}Ca$ values changed towards lower values over the last 500 Ma with significantly low values in the last 100–200 Ma (Fig. A. 1a). Recycling of such crustal carbonates with unusually low $\delta^{44/40}Ca$ could facilitate the modification of the $\delta^{44/40}Ca$ values of Earth's upper mantle. The lowering in $\delta^{44/40}Ca$ values of marine carbonates could

be triggered by events such as the Siberian Trap volcanism at the Permian-Triassic boundary (e.g., Campbell et al., 1992; Payne et al., 2010; Wang et al., 2019b).

Geochemical and Nd isotopic compositions of komatiites and basalts suggest that global subduction processes and plume activity may have initiated as early as ~3.2 Ga (El Dien et al., 2019, 2020). However, $^{87}Sr/^{86}Sr$ of global carbonatites suites (this study and Rukhlov et al., 2015) in association with their $\varepsilon_{Nd(t)}$, $^{206}Pb/^{204}Pb$ and $^{208}Pb/^{204}Pb$ ratios (Bell and Simonetti, 2010; Rukhlov et al., 2015) suggest that these isotopic signatures were more widely spread with pronounced effect of recycling in last 300 million years, while having relatively constricted values for carbonatites of age older than 300 Ma. These observations suggest that carbonatites older than 300 Ma were derived primarily from a mantle source with limited involvement of recycled carbonate components. Such observations are consistent with the $\delta^{44/40}Ca$ values presented in this study for carbonatites older than 300 Ma, which suggests that recycling events were sporadic in the geological past. However, the overall higher $\delta^{44/40}Ca$ values for Precambrian carbonates, which are similar to the estimated value of the BSE, further constrain our ability to infer the role of carbonate recycling in modifying the compositions of the Precambrian carbonatites using Ca isotopes. The same applies for the $^{87}Sr/^{86}Sr$ signatures of Precambrian carbonatites as the Sr isotope composition of seawater in the Archean was heavily buffered by mantle Sr.

## 5. CONCLUSIONS

(1) A majority of carbonatites (whole rock as well as calcite separates) older than 300 Ma, with the exception of carbonatites from the Phalaborwa complex of South Africa and the Neoproterozoic carbonatites of south India, define a restricted range in $\delta^{44/40}Ca$ and $^{87}Sr/^{86}Sr$, which overlaps with the composition estimated for the BSE. The BSE-like $\delta^{44/40}Ca$ along with the $^{87}Sr/^{86}Sr$ for majority of the older carbonatites suggest that recycling of crustal materials was not widespread in the geological past.

(2) Carbonatites (whole rock as well as calcite separates) younger than 300 Ma show significant variations in their $\delta^{44/40}Ca$ values, with many samples displaying $\delta^{44/40}Ca$ values lower than that estimated for the BSE. These low $\delta^{44/40}Ca$ values cannot be explained by post-emplacement low-temperature processes, crustal contamination, wall-rock interaction, hydrothermal alteration, and partial melting. Additionally, these younger carbonatites also show a large spread in their $^{87}Sr/^{86}Sr$ with values trending towards more radiogenic compositions. The combined Ca and Sr isotopic signatures of the younger carbonatites are attributed to the presence of recycled carbonates, characterized by low $\delta^{44/40}Ca$ values and radiogenic $^{87}Sr/^{86}Sr$, in their mantle source regions. Model calculations, based on $\delta^{44/40}Ca$ values and $^{87}Sr/^{86}Sr_{(t)}$ ratios of the mantle peridotite and eclogite sources and marine carbonates of different ages, suggest that the $\delta^{44/40}Ca$ and $^{87}Sr/^{86}Sr$ for most of the younger carbonatites (<300 Ma) examined here can be explained by the presence of 4–10 wt% recycled crustal carbonates in the mantle source of these rocks. Significant crustal recycling signature in carbonatites younger than 300 Ma is attributed to an increased subduction flux and high rate of plate convergence associated with the initiation of breakup of the Pangea supercontinent, which was also accompanied by increased plume activity. The subduction of compositionally distinct marine carbonates with relatively low $\delta^{44/40}Ca$ values, triggered by large events such as the Siberian Traps volcanism at ~250 Ma ago, could have further accentuated the low $\delta^{44/40}Ca$ for carbonatites younger than 300 Ma.

## Declaration of Competing Interest

The authors declare that they have no known competing financial interests or personal relationships that could have appeared to influence the work reported in this paper.

### ACKNOWLEDGEMENTS

RC acknowledges funding from DST, India (SR/FTP/ES-72/2012 and CRG/2018/004254). Some of the whole-rock samples were provided by the Harvard Museum of Natural History, Profs. Prosenjit Ghosh, and Rajesh Srivastava. We thank Shichun Huang, Zaicong Wang, and a third anonymous reviewer and the Associate Editor Dmitri Ionov for their comments and suggestions.

## APPENDIX A. SUPPLEMENTARY MATERIAL

Supplementary data to this article can be found online at https://doi.org/10.1016/j.gca.2021.05.046.

## REFERENCES

Ackerman L., Magna T., Rapprich V., Upadhyay D., Krátký O., Čejková B., Erban V., Kochergina Y. V. and Hrstka T. (2017) Contrasting petrogenesis of spatially related carbonatites from Samalpatti and Sevattur, Tamil Nadu, India. *Lithos* **284–285**, 257–275.

Ackerman L., Polák L., Magna T., Rapprich V., Ďurišová J. and Upadhyay D. (2019) Highly siderophile element geochemistry and Re–Os isotopic systematics of carbonatites: insights from Tamil Nadu, India. *Earth Planet. Sci. Lett.* **520**, 175–187.

Amini M., Eisenhauer A., Böhm F., Holmden C., Kreissig K., Hauff F. and Jochum K. P. (2009) Calcium isotopes ($\delta^{44/40}Ca$) in MPI-DING reference glasses, USGS rock powders and various rocks: evidence for Ca isotope fractionation in terrestrial silicates. *Geostand. Geoanalytic. Res.* **33**, 231–247.

Amsellem E., Moynier F., Bertrand H., Bouyon A., Mata M., Tappe S. and Day J. M. D. (2020) Calcium isotopic evidence for the mantle sources of carbonatites. *Sci. Adv.* **6**, eaba3269.

Antonelli M. A. and Simon J. I. (2020) Calcium isotopes in high-temperature terrestrial processes. *Chem. Geol.* **548** 119651.

Antonelli M. A., DePaolo D. J., Chacko T., Grew E. S. and Rubatto D. (2019) Radiogenic Ca isotopes confirm post-

formation K depletion of lower crust. *Geochem. Perspect. Lett.* **9**, 43–48.

Banerjee A. and Chakrabarti R. (2019) A geochemical and Nd, Sr and stable Ca isotopic study of carbonatites and associated silicate rocks from the~ 65 Ma old Ambadongar carbonatite complex and the Phenai Mata igneous complex, Gujarat, India: implications for crustal contamination, carbonate recycling, hydrothermal alteration and source-mantle mineralogy. *Lithos* **326**, 572–585.

Banerjee A., Chakrabarti R. and Mandal S. (2016) Geochemical anatomy of a spheroidally weathered diabase. *Chem. Geol.* **440**, 124–138.

Basu S. and Murty S. V. S. (2015) Nitrogen and argon in Sung Valley and Ambadongar carbonatite complexes: evidence of incomplete homogenization of mantle and recycled components. *J. Asian Earth Sci.* **107**, 53–61.

Bell K. and Blenkinsop J. (1987) Archean depleted mantle: Evidence from Nd and Sr initial isotopic ratios of carbonatites. *Geochim. Cosmochim. Acta* **51**, 291–298.

Bell K. and Blenkinsop J. (1989) Neodymium and strontium isotope geochemistry of carbonatites. In *Carbonatites* (ed. K. Bell). Unwin Hyman, New York, pp. 278–300.

Bell K. and Simonetti A. (2010) Source of parental melts to carbonatites–critical isotopic constraints. *Mineral. Petrol.* **98**, 77–89.

Bell K. and Tilton G. R. (2001) Nd, Pb and Sr Isotopic Compositions of East African Carbonatites: evidence for Mantle Mixing and Plume Inhomogeneity. *J. Petrol.* **42**, 1927–1945.

Bell K., Blenkinsop J., Cole T. J. S. and Menagh D. P. (1982) Evidence from Sr isotopes for long-lived heterogeneities in the upper mantle. *Nature* **298**, 251–253.

Bell K., Lavecchia G. and Rosatelli G. (2013) Cenozoic Italian magmatism – Isotope constraints for possible plume-related activity. *J. South Am. Earth Sci.* **41**, 22–40.

Bizimis M., Salters V. J. M. and Dawson J. B. (2003) The brevity of carbonatite sources in the mantle: evidence from Hf isotopes. *Contrib. Mineral. Petrol.* **145**, 281–300.

Bizzarro M., Simonetti A., Stevenson R. K. and David J. (2002) Hf isotope evidence for a hidden mantle reservoir. *Geology* **30**, 771–774.

Blättler C. L., Henderson G. M. and Jenkyns H. C. (2012) Explaining the Phanerozoic Ca isotope history of seawater. *Geology* **40**, 843–846.

Blättler C. L. and Higgins J. A. (2017) Testing Urey's carbonate–silicate cycle using the calcium isotopic composition of sedimentary carbonates. *Earth Planet. Sci. Lett.* **479**, 241–251.

Bolhar R., Whitehouse M. J., Milani L., Magalhães N., Golding S. D., Bybee G., LeBras L. and Bekker A. (2020) Atmospheric S and lithospheric Pb in sulphides from the 2.06 Ga Phalaborwa phoscorite-carbonatite Complex, South Africa. *Earth Planet. Sci. Lett.* **530** 115939.

Brey G. P., Bulatov V. K., Girnis A. V. and Lahaye Y. (2008) Experimental melting of carbonated peridotite at 6–10 GPa. *J. Petrol.* **49**, 797–821.

Campbell I. H., Czamanske G. K., Fedorenko V. A., Hill R. I. and Stepanov V. (1992) Synchronism of the Siberian traps and the permian-triassic boundary. *Science* **258**, 1760–1763.

Castorina F., Stoppa F., Cundari A. and Barbieri M. (2000) An enriched mantle source for Italy's melilitite-carbonatite association as inferred by its Nd-Sr isotope signature. *Mineral. Mag.* **64**, 625–639.

Chandra J., Paul D., Stracke A., Chabaux F. and Granet M. (2019) The origin of carbonatites from amba dongar within the Deccan large igneous Province. *J. Petrol.* **60**, 1119–1134.

Chen W. and Simonetti A. (2013) In-situ determination of major and trace elements in calcite and apatite, and U-Pb ages of apatite from the Oka carbonatite complex: insights into a complex crystallization history. *Chem. Geol.* **353**, 151–172.

Chen W. and Simonetti A. (2014) Evidence for the multi-stage petrogenetic history of the Oka carbonatite complex (Québec, Canada) as recorded by perovskite and apatite. *Minerals* **4**, 437–476.

Chen C., Dai W., Wang Z., Liu Y., Li M., Becker H. and Foley S. F. (2019) Calcium isotope fractionation during magmatic processes in the upper mantle. *Geochim. Cosmochim. Acta* **249**, 121–137.

Çimen O., Kuebler C., Monaco B., Simonetti S. S., Corcoran L., Chen W. and Simonetti A. (2018) Boron, carbon, oxygen and radiogenic isotope investigation of carbonatite from the Miaoya complex, central China: evidences for late-stage REE hydrothermal event and mantle source heterogeneity. *Lithos* **322**, 225–237.

Cimen O., Kuebler C., Simonetti S. S., Corcoran L., Mitchell R. and Simonetti A. (2019) Combined boron, radiogenic (Nd, Pb, Sr), stable (C, O) isotopic and geochemical investigations of carbonatites from the Blue River Region, British Columbia (Canada): implications for mantle sources and recycling of crustal carbon. *Chem. Geol.* **529**, 19240.

Collins W. J. (2003) Slab pull, mantle convection, and Pangaean assembly and dispersal. *Earth Planet. Sci. Lett.* **205**, 225–237.

Dasgupta R. and Hirschmann M. M. (2006) Melting in the Earth's deep upper mantle caused by carbon dioxide. *Nature* **440**, 659–662.

Dasgupta R., Hirschmann M. M. and Smith N. D. (2007) Partial melting experiments of peridotite+ $CO_2$ at 3 GPa and genesis of alkalic ocean island basalts. *J. Petrol.* **48**, 2093–2124.

Dasgupta R., Hirschmann M. M., McDonough W. F., Spiegelman M. and Withers A. C. (2009) Trace element partitioning between garnet lherzolite and carbonatite at 6.6 and 8.6 GPa with applications to the geochemistry of the mantle and of mantle-derived melts. *Chem. Geol.* **262**, 57–77.

Dobson D. P., Jones A. P., Rabe R., Sekine T., Kurita K., Taniguchi T., Kondo T., Kato T., Shimomura O. and Urakawa S. (1996) In-situ measurement of viscosity and density of carbonate melts at high pressure. *Earth Planet. Sci. Lett.* **143**, 207–215.

D'Orazio M., Innocenti F., Tonarini S. and Doglioni C. (2007) Carbonatites in a subduction system: The Pleistocene alvikites from Mt. Vulture (southern Italy). *Lithos* **98**, 313–334.

Doucelance R., Hammouda T., Moreira M. and Martins J. C. (2010) Geochemical constraints on depth of origin of oceanic carbonatites: the Cape Verde case. *Geochimi Cosmochim. Acta* **74**, 7261–7282.

East M., Müller R. D., Williams S., Zahirovic S. and Heine C. (2020) Subduction history reveals Cretaceous slab superflux as a possible cause for the mid-Cretaceous plume pulse and superswell events. *Gond. Res.* **79**, 125–139.

El Dien H. G., Doucet L. S. and Li Z. X. (2019) Global geochemical fingerprinting of plume intensity suggests coupling with the supercontinent cycle. *Nat. Comm.* **10**, 1–7.

El Dien H. G., Doucet L. S., Murphy J. B. and Li Z. X. (2020) Geochemical evidence for a widespread mantle re-enrichment 3.2 billion years ago: implications for global-scale plate tectonics. *Sci. Rep.* **10**, 1–7.

Ernst R. E. (2014) *Large Igneous Provinces, Large Igneous Provinces*. Cambridge University Press, Cambridge.

Ernst R. E. and Bell K. (2010) Large igneous provinces (LIPs) and carbonatites. *Mineral. Petrol.* **98**, 55–76.

Fantle M. S. and Tipper E. T. (2014) Calcium isotopes in the global biogeochemical Ca cycle: implications for development of a Ca isotope proxy. *Earth-Sci. Rev.* **129**, 148–177.

Farkas J., Buhl D., Blenkinsop J. and Veizer J. (2007a) Evolution of the oceanic calcium cycle during the late Mesozoic: evidence from $\delta^{44/40}$Ca of marine skeletal carbonates. *Earth Planet. Sci. Lett.* **253**, 96–111.

Farkaš J., Bohm F., Wallmann K., Blenkinsop J., Eisenhauer A., Geldren R. V., Munnecke A., Voigt S. and Veizer J. (2007b) Calcium isotope record of phanerozoic oceans: implications for chemical evolution of seawater and its causative mechanisms. *Geochim. Cosmochim. Acta* **71**, 5117–5134.

Farkaš J., Déjeant A., Novák M. and Jacobsen S. B. (2011) Calcium isotope constraints on the uptake and sources of Ca2+ in a base-poor forest: a new concept of combining stable ($\delta^{44/42}$Ca) and radiogenic (εCa) signals. *Geochim. Cosmochim. Acta* **75**, 7031–7046.

Feng L., Zhou L., Yang L., DePaolo D. J., Tong S.-Y., Liu Y.-S., Owens T. L. and Gao S. (2017) Calcium isotopic compositions of sixteen USGS reference materials. *Geostand. Geoanalytic. Res.* **41**, 93–106.

Freestone I. C. and Hamilton D. L. (1980) The role of liquid immiscibility in the genesis of carbonatites- an experimental study. *Contrib. Mineral. Petrol.* **73**, 105–117.

Halama R., McDonough W. F., Rudnick R. L. and Bell K. (2008) Tracking the lithium isotopic evolution of the mantle using carbonatites. *Earth Planet. Sci. Lett.* **265**, 726–742.

He Y., Wang Y., Zhu C., Huang S. and Li S. (2017) Mass-independent and mass-dependent Ca isotopic compositions of thirteen geological reference materials measured by thermal ionisation mass spectrometry. *Geostand. Geoanalytic. Res.* **41**, 283–302.

Hoernle K., Tilton G., Le Bas M. J., Duggen S. and Garbe-Schönberg D. (2002) Geochemistry of oceanic carbonatites compared with continental carbonatites: mantle recycling of oceanic crustal carbonate. *Contrib. Mineral. Petrol.* **142**, 520–542.

Hofmann A. W. (1997) Mantle geochemistry: the message from oceanic volcanism. *Nature* **385**, 219–229.

Hounslow M. W., Domeier M. and Biggin A. J. (2018) Subduction flux modulates the geomagnetic polarity reversal rate. *Tectonophysics* **742–743**, 34–49.

Huang F, Chen Z, Wenzhong W, Jinting K and Zhongqing W (2019) First-principles calculations of equilibrium Ca isotope fractionation: Implications for oldhamite formation and evolution of lunar magma ocean. *Earth Planet. Sci. Lett.* **510**, 153–160.

Huang S., Farkaš J. and Jacobsen S. B. (2010a) Calcium isotopic fractionation between clinopyroxene and orthopyroxene from mantle peridotites. *Earth Planet. Sci. Lett.* **292**, 337–344.

Huang F., Chakraborty P., Lundstrom C. C., Holmden C., Glessner J. J. G., Kieffer S. W. and Lesher C. E. (2010b) Isotope fractionation in silicate melts by thermal diffusion. *Nature* **464**, 396–400.

Huang S., Farkaš J. and Jacobsen S. B. (2011) Stable calcium isotopic compositions of Hawaiian shield lavas: evidence for recycling of ancient marine carbonates into the mantle. *Geochim. Cosmochim. Acta* **75**, 4987–4997.

Hulett S. R. W., Simonetti A., Rasbury E. T. and Hemming N. G. (2016) Recycling of subducted crustal components into carbonatite melts revealed by boron isotopes. *Nat. Geosci.* **9**, 904–908.

Ionov D. A., Qi Y.-H., Kang J.-T., Golovin A. V., Oleinikov O. B., Zheng W., Anbar A. D., Zhang Z.-F. and Huang F. (2019) Calcium isotopic signatures of carbonatite and silicate metasomatism, melt percolation and crustal recycling in the lithospheric mantle. *Geochim. Cosmochim. Acta* **248**, 1–13.

Jones A. P., Genge M. and Carmody L. (2013) Carbonate melts and carbonatites. *Rev. Mineral. Geochem.* **75**, 289–322.

Jung S. G., Choi S. H., Ji K. H., Ryu J. S. and Lee D. C. (2019) Geochemistry of volcanic rocks from Oldoinyo Lengai, Tanzania: Implications for mantle source lithology. *Lithos* **350–351** 105223.

Kaminsky F. V., Ryabchikov I. D. and Wirth R. (2016) A primary natrocarbonatitic association in the Deep Earth. *Mineral. Petrol.* **110**, 387–398.

Kang J.-T., Ionov D. A., Liu F., Zhang C.-L., Golovin A. V., Qin L.-P., Zhang Z.-F. and Huang F. (2017) Calcium isotopic fractionation in mantle peridotites by melting and metasomatism and Ca isotope composition of the Bulk Silicate Earth. *Earth Planet. Sci. Lett.* **474**, 128–137.

Kang J.-T., Zhou C., Huang J. Y., Hao Y. T., Liu F., Zhu H. L., Zhang Z. F. and Huang F. (2020) Diffusion-driven Ca-Fe isotope fractionations in the upper mantle: Implications for mantle cooling and melt infiltration. *Geochim. Cosmochim. Acta* **290**, 41–58.

Kuebler C., Simonetti A., Chen W. and Simonetti S. S. (2020) Boron isotopic investigation of the Bayan Obo carbonatite complex: Insights into the source of mantle carbon and hydrothermal alteration. *Chem. Geol.* **557** 119859.

Kumar A., Charan S. N., Gopalan K. and Macdougall J. D. (1998) A Long-Lived Enriched Mantle Source for Two Proterozoic Carbonatite Complexes from Tamil Nadu,, Southern India. *Geochim. Cosmochim. Acta* **62**, 515–523.

Li M., Lei Y., Feng L., Wang Z., Belshaw N. S., Hu Z., Liu Y., Zhou L., Chen H. and Chai X. (2018) High-precision Ca isotopic measurement using a large geometry high resolution MC-ICP-MS with a dummy bucket. *J. Anal. Atom. Spec.* **33**, 1707–1719.

Li W.-Y., Yu H.-M., Xu J., Halama R., Bell K., Nan X.-Y. and Huang F. (2020) Barium isotopic composition of the mantle: Constraints from carbonatites. *Geochim. Cosmochim. Acta* **278**, 235–243.

Liu F., Li X., Wang G., Liu Y., Zhu H., Kang J., Huang F., Sun W., Xia X. and Zhang Z. (2017) Marine carbonate component in the mantle beneath the southeastern Tibetan Plateau: evidence from magnesium and calcium isotopes. *J. Geophys. Res. Solid Earth* **122**, 9729–9744.

Liu F., Li X., An Y. J., Li J. and Zhang Z. F. (2019) Calcium isotope ratio ($\delta^{44/40}$Ca) measurements of ca-dominated minerals and rocks without column chemistry using the double-spike technique and thermal ionisation mass spectrometry. *Geostand. Geoanalytic. Res.* **43**, 509–517.

Marschall H. R., Wanless V. D., Shimizu N., von Strandmann P. A. P., Elliott T. and Monteleone B. D. (2017) The boron and lithium isotopic composition of mid-ocean ridge basalts and the mantle. *Geochim. Cosmochim. Acta* **207**, 102–138.

McDonough W. F. and Sun S. S. (1995) The composition of the Earth. *Chem. Geol.* **120**, 223–253.

Mills R. D., Simon J. I. and DePaolo D. J. (2018) Calcium and neodymium radiogenic isotopes of igneous rocks: Tracing crustal contributions in felsic magmas related to super-eruptions and continental rifting. *Earth Planet. Sci. Lett.* **495**, 242–250.

Mondal S. and Chakrabarti R. (2018) A novel sample loading method and protocol for monitoring sample fractionation for high precision Ca stable isotope ratio measurements using double-spike TIMS. *J. Anal. At. Spec.* **33**, 141–150.

Nelson D. R., Chivas A. R., Chappell B. W. and McCulloch M. T. (1988) Geochemical and isotopic systematics in carbonatites and implications for the evolution of ocean-island sources. *Geochim. Cosmochim. Acta* **52**, 1–17.

Palme H. and O'Neill H. D. C. (2014) Cosmochemical estimates of mantle composition. In: Carlson, R.W. (eds) Treatise on geochemistry, 3, 1–39.

Pandit M. K., Sial A. N., Sukumaran G. B., Pimentel M. M., Ramasamy A. K. and Ferreira V. P. (2002) Depleted and enriched mantle sources for Paleo- and Neoproterozoic carbonatites of southern India: Sr, Nd, C-O isotopic and geochemical constraints. *Chem. Geol.* **189**, 69–89.

Payne J. L., Turchyn A. V., Paytan A., DePaolo D. J., Lehrmann D. J., Yu M. and Wei J. (2010) Calcium isotope constraints on the end-Permian mass extinction. *Proc. Nat. Aca. Sci.* **107**, 8543–8548.

Peretyazhko I. S. and Savina E. A. (2010) Tetrad effects in the rare earth element patterns of granitoid rocks as an indicator of fluoride-silicate liquid immiscibility in magmatic systems. *Petrology* **18**, 514–543.

Ray J. S. and Ramesh R. (2006) Stable carbon and oxygen isotopic compositions of Indian carbonatites. *Int. Geol. Rev.* **48**, 17–45.

Ray J. S., Ramesh R. and Pande K. (1999) Carbon isotopes in Kerguelen plume-derived carbonatites: evidence for recycled inorganic carbon. *Earth Planet. Sci. Lett.* **170**, 205–214.

Richter F. M., Watson E. B., Mendybaev R. A., Teng F. Z. and Janney P. E. (2008) Magnesium isotope fractionation in silicate melts by chemical and thermal diffusion. *Geochim. Cosmochim. Acta* **72**, 206–220.

Rudnick R. L. and Gao S. (2004) Composition of the continental crust. *Treatise Geochem.* **3**, 1–64.

Rukhlov A. S., Bell K. and Amelin Y. (2015) Carbonatites, isotopes and evolution of the subcontinental mantle: an overview. In: Symp. Crit. Strateg. Mat. 39–64 (British Columbia Geological Survey Paper 2015–3, BC Geological Survey).

Salters V. J. M. and Stracke A. (2004) Composition of the depleted mantle. *Geochem. Geophy. Geosyst.* **5**.

Schleicher H., Kramm U., Pernicka E., Schidlowski M., Schmidt F., Subramanian V., Todt W. and Viladkar S. G. (1998) Enriched Subcontinental Upper Mantle beneath Southern India: Evidence from Pb, Nd, Sr, and C-O Isotopic Studies on Tamil Nadu Carbonatites. *J. Petrol.* **39**, 1765–1785.

Shaw A. M., Hauri E. H., Behn M. D., Hilton D. R., Macpherson C. G. and Sinton J. M. (2012) Long-term preservation of slab signatures in the mantle inferred from hydrogen isotopes. *Nat. Geosc.* **5**, 224–228.

Simonetti A., Bell K. and Viladkar S. G. (1995) Isotopic data from the Amba Dongar Carbonatite Complex, west-central India: Evidence for an enriched mantle source. *Chem. Geol.* **122**, 185–198.

Simonetti A., Goldstein S. L., Schmidberger S. S. and Viladkar S. G. (1998) Geochemical and Nd, Pb, and Sr isotope data from Deccan alkaline complexes-inferences for mantle sources and plume-lithosphere interaction. *J. Petrol.* **39**, 1847–1864.

Smart K. A., Tappe S., Woodland A. B., Greyling D. R., Harris C. and Gussone N. (2021) Constraints on Archean crust recycling and the origin of mantle redox variability from the $\delta^{44/40}$Ca–$\delta^{18}$O–f$O_2$ signatures of cratonic eclogites. *Earth Planet. Sci. Lett.* **556** 116720.

Srivastava R. K., Heaman L. M., Sinha A. K. and Shihua S. (2005) Emplacement age and isotope geochemistry of Sung Valley alkaline–carbonatite complex, Shillong Plateau, northeastern India: implications for primary carbonate melt and genesis of the associated silicate rocks. *Lithos* **81**, 33–54.

Stracke A., Bizimis M. and Salters V. J. M. (2003) Recycling oceanic crust: Quantitative constraints. *Geochem. Geophys. Geosyst.* **4**.

Stracke A., Hofmann A. W. and Hart S. R. (2005) FOZO, HIMU, and the rest of the mantle zoo. *Geochem. Geophys. Geosyst.* **6**.

Sun S. S. and McDonough W. F. (1989) Chemical and isotopic systematics of oceanic basalts: implications for mantle composition and processes. *Geol. Soc. London Sp. Pub.* **42**, 313–345.

Sun J., Zhu X. K., Belshaw N. S., Chen W., Doroshkevich A. G., Luo W. J., Song W. L., Chen B. B., Cheng Z. G., Li Z. H. and Wang Y. (2021) Ca isotope systematics of carbonatites: Insights into carbonatite source and evolution. *Geochem. Persp. Lett.* **17**, 11–15.

Veizer J. and Compston W. (1976) $^{87}$Sr/$^{86}$Sr in Precambrian carbonates as an index of crustal evolution. *Geochim. Cosmochim. Acta* **40**, 905–914.

Veksler I. V., Petibon C., Jenner G. A., Dorfman A. M. and Dingwell D. B. (1998) Trace element partitioning in immiscible silicate–carbonate liquid systems: an initial experimental study using a centrifuge autoclave. *J. Petrol.* **39**, 2095–2104.

Veksler I. V., Dorfman A. M., Dulski P., Kamenetsky V. S., Danyushevsky L. V., Jeffries T. and Dingwell D. B. (2012) Partitioning of elements between silicate melt and immiscible fluoride, chloride, carbonate, phosphate and sulfate melts, with implications to the origin of natrocarbonatite. *Geochim. Cosmochim. Acta* **79**, 20–40.

Wang Y., He Y., Wu H., Zhu C., Huang S. and Huang J. (2019a) Calcium isotope fractionation during crustal melting and magma differentiation: granitoid and mineral-pair perspectives. *Geochim. Cosmochim. Acta* **259**, 37–52.

Wang J., Jacobson A. D., Zhang H., Ramezani J., Sageman B. B., Hurtgen M. T., Bowring S. A. and Shen S.-Z. (2019b) Coupled $\delta^{44/40}$Ca, $\delta^{88/86}$Sr, and $^{87}$Sr/$^{86}$Sr geochemistry across the end-Permian mass extinction event. *Geochim. Cosmochim. Acta* **262**, 143–165.

Willbold M. and Stracke A. (2006) Trace element composition of mantle end-members: Implications for recycling of oceanic and upper and lower continental crust. *Geochem. Geophys. Geosyst.* **7**.

Willbold M. and Stracke A. (2010) Formation of enriched mantle components by recycling of upper and lower continental crust. *Chem. Geol.* **276**, 188–197.

Woolley A. R. (1982) A discussion of carbonatite evolution and nomenclature, and the generation of sodic and potassic fenites. *Mineral. Mag.* **46**, 13–17.

Woolley A. R. and Church A. A. (2005) Extrusive carbonatites: A brief review. *Lithos* **85**, 1–14.

Woolley A. R. and Kjarsgaard B. A. (2008) Paragenetic types of carbonatite as indicated by the diversity and relative abundances of associated silicate rocks: evidence from a global database. *Can. Mineral.* **46**, 741–752.

Workman R. K., Hart S. R., Jackson M., Regelous M., Farley K. A., Blusztajn J., Kurz M. and Staudigel H. (2004) Recycled metasomatized lithosphere as the origin of the Enriched Mantle II (EM2) end-member: Evidence from the Samoan Volcanic Chain. *Geochem. Geophys. Geosyst.* **5**.

Wu F.-Y., Yang Y.-H., Li Q.-L., Mitchell R. H., Dawson J. B., Brandl G. and Yuhara M. (2011) In situ determination of U-Pb ages and Sr–Nd–Hf isotopic constraints on the petrogenesis of the Phalaborwa carbonatite Complex, South Africa. *Lithos* **127**, 309–322.

Yaxley G. M., Ghosh S., Kiseeva E. S., Mallik A., Spandler C., Thomson A. R. and Walter M. J. (2020) $CO_2$-rich melts in Earth. In *Deep Carbon: Past to Present* (eds. B. N. Orcutt, I. Daniel and R. Dasgupta). Cambridge University Press, Cambridge, UK, pp. 129–162.

Zaitsev A. and Keller J. (2006) Mineralogical and chemical transformation of Oldoinyo Lengai natrocarbonatites, Tanzania. *Lithos* **91**, 191–207.

Zhang H., Wang Y., He Y., Teng F. Z., Jacobsen S. B., Helz R. T., Marsh B. D. and Huang S. (2018) No measurable calcium

isotopic fractionation during crystallization of Kilauea Iki lava lake. *Geochem. Geophy. Geosyst.* **19**, 3128–3139.

Zhao X., Zhang Z., Huang S., Liu Y., Li X. and Zhang H. (2017) upled extremely light Ca and Fe isotopes in peridotites. *Geochim. Cosmochim. Acta* **208**, 368–380.

Zhu H., Liu F., Li X., Wang G., Zhang Z. and Sun W. (2018) Calcium isotopic compositions of normal mid-ocean ridge basalts from the southern Juan de Fuca Ridge. *J. Geophys. Res. Solid Earth* **123**, 1303–1313.

Zhu H., Liu F., Li X., An Y., Nan X., Du L., Huang F., Sun W. and Zhang Z. (2020a) Significant $\delta^{44/40}$Ca variations between carbonate- and clay-rich marine sediments from the Lesser Antilles forearc and implications for mantle heterogeneity. *Geochim. Cosmochim. Acta* **276**, 239–257.

Zhu H., Du L., Li X., Zhang Z. and Sun W. (2020b) Calcium isotopic fractionation during plate subduction: Constraints from back-arc basin basalts. *Geochim. Cosmochim. Acta* **270**, 379–393.

*Associate editor:* Dmitri A. Ionov